

# FaIRv2.0.0: a generalised impulse-response model for climate uncertainty and future scenario exploration

Nicholas J. Leach<sup>1</sup>, Stuart Jenkins<sup>1</sup>, Zebedee Nicholls<sup>2,3</sup>, Christopher J. Smith<sup>4,5</sup>, John Lynch<sup>1</sup>, Michelle Cain<sup>1</sup>, Tristram Walsh<sup>1</sup>, Bill Wu<sup>1</sup>, Junichi Tsutsui<sup>6</sup>, and Myles R. Allen<sup>1,7</sup>

<sup>1</sup>Department of Physics, Atmospheric, Oceanic, and Planetary Physics, University of Oxford, United Kingdom.

<sup>2</sup>Australian–German Climate and Energy College, University of Melbourne, Australia.

<sup>3</sup>School of Earth Sciences, University of Melbourne, Australia.

<sup>4</sup>School of Earth and Environment, University of Leeds, Leeds, UK.

<sup>5</sup>International Institute for Applied Systems Analysis, Laxenburg, Austria.

<sup>6</sup>Environmental Science Laboratory, Central Research Institute of Electric Power Industry, Abiko-shi, Japan.

<sup>7</sup>Environmental Change Institute, University of Oxford, Oxford, UK.

**Correspondence:** Nicholas J. Leach (nicholas.leach@stx.ox.ac.uk)

**Abstract.** Here we present an update to the FaIR model for use in probabilistic future climate and scenario exploration, integrated assessment, policy analysis and education. In this update we have focussed on identifying a minimum level of structural complexity in the model. The result is a set of six equations, five of which correspond to the standard Impulse Response model used for greenhouse gas (GHG) metric calculations in the IPCC’s fifth assessment report, plus one additional 5 physically-motivated additional equation to represent state-dependent feedbacks on the response timescales of each greenhouse gas cycle. This additional equation is necessary to reproduce non-linearities in the carbon cycle apparent in both Earth System Models and observations. These six equations are transparent and sufficiently simple that the model is able to be ~~written in~~ reported into standard tabular data analysis packages, such as Excel; increasing the potential user base considerably. However, we demonstrate that the equations are flexible enough to be tuned to emulate the behaviour of several key processes within 10 more complex models from CMIP6. The model is exceptionally quick to run, making it ideal for integrating large probabilistic ensembles. We apply a constraint based on the current estimates of the global warming trend to a one million member ensemble, using the constrained ensemble to make scenario dependent projections and infer ranges for properties of the climate system. Through these analyses, we reaffirm that simple climate models (unlike more complex models) are not themselves intrinsically biased “hot” or “cold”: it is the choice of parameters and how those are selected that determines the model response, something 15 that appears to have been misunderstood in the past. This updated FaIR model is able to reproduce the global climate system response to GHG and aerosol emissions with sufficient accuracy to be useful in a wide range of applications; and therefore could be used as a lowest common denominator model to provide consistency in different contexts. The fact that FaIR can be written down in just six equations greatly aids transparency in such contexts.

*Copyright statement.* © Author(s) 2019. This work is distributed under the Creative Commons Attribution 4.0 License.

20 **1 Introduction**

Earth System Models (ESMs) are vital tools for providing insight into the drivers behind Earth's climate system, as well as projecting impacts of future emissions. Large scale multi-model studies, such as the Coupled Model Intercomparison Projects (Eyring et al., 2016; Taylor et al., 2012, CMIPs), have been used in many reports to produce projections of what the future climate may look like based on a range of different concentration scenarios, with associated emission scenarios and socio-economic narratives quantified by Integrated Assessment Models (IAMs). In addition to simulating both the past and possible future climates, these CMIPs extensively use idealised experiments to try to determine some of the key properties of the climate system, such as the equilibrium climate sensitivity [ECS, Collins et al. (2013)], or the transient climate response to cumulative carbon emissions (Allen et al., 2009, TCRE).

30 While ESMs are integral to our current understanding of how the climate system responds to GHG and aerosol emissions, and provide the most comprehensive projections of what a future world might look like, they are so computationally expensive that only a limited set of experiments are able to be run during a CMIP. This constraint on the quantity of experiments necessitates the use of simpler models to provide probabilistic assessments and explore additional experiments and scenarios. These models, often referred to as simple climate models (SCMs), are typically designed to emulate the response of more 35 complex models. In general, they are able to simulate the globally averaged emission → concentration → radiative forcing → temperature response pathway, and can be tuned to emulate an individual ESM (or multi-model-mean). In general, SCMs are considerably less complex than ESMs: while ESMs are three dimensional, gridded, and explicitly represent dynamical and physical processes, therefore outputting many hundreds of variables, SCMs tend to be globally averaged (or cover large regions), and parameterise many processes, resulting in many fewer output variables. This reduction in complexity means that 40 SCMs are much quicker than ESMs in terms of runtime: most SCMs can run tens of thousands of years of simulation per minute on an “average” personal computer, whereas ESMs may take several hours to run a single year on hundreds of supercomputer processors; and are much smaller in terms of the number of lines of code: SCMs tend to be on the order of thousands of lines, ESMs can be up to a million lines (Alexander and Easterbrook, 2015).

45 **Several** There are many simple climate models ~~are available, such as the two~~ (Nicholls et al., 2020a) that have been in use by the climate science and integrated assessment modelling communities for decades. Of particular note are MAGICC (Meinshausen et al., 2011a), which has dominated SCM usage within integrated assessment models, and FaIR<sup>1</sup> (Smith et al., 2018); both of which were used in the Intergovernmental Panel on Climate Change (IPCC) Special Report on 1.5°C warming (IPCC, 2018, SR15): ~~FaIR v1.3 (Smith et al., 2018)~~ and ~~MAGICC6 (Meinshausen et al., 2011a)~~. However, while these models are “simple” in comparison to the ESMs they emulate, they are often ~~still not so simple as not simple enough~~ to allow new users to gain enough familiarity with the underlying equations to understand their behaviour without significant effort. This learning curve reduces 50

---

<sup>1</sup>We refer to the FaIR model in general as “FaIR”, to the version presented in this text as “FaIRv2.0.0”, and to the specific implementation used to create the figures as “FaIRv2.0.0-alpha” throughout.

their uptake by the wider community, and has resulted in different research groups generally using the single model that they are most familiar with (Nicholls et al., 2020a) from the wide range of SCMs. In the past, this has led to ~~a~~-different simple models being used by different working groups in major reports, reducing the consistency of the overall work. We believe one key step towards a transparent and coherent process in IPCC Assessments would be ~~the use of~~ to use at least one common SCM as widely as possible throughout all working groups, allowing results to be directly comparable. Such use would provide additional context alongside domain specific models. For this to be realised, an SCM that is both easy to understand and adapt is required.

An important innovation of the IPCC 5th Assessment Report (Myhre et al., 2013) was the introduction of a ~~fully~~ transparent set of equations (the AR5-IR model) for use in the calculation of GHG metrics. However, that model was not quite adequate to reproduce the evolution of the integrated impulse response to emissions over time, due to the lack of non-linearity in the carbon cycle. The Finite amplitude Impulse Response (FaIR) model v1.0 (Millar et al., 2017) introduced a state-dependence to the AR5-IR carbon cycle. This state-dependent carbon cycle was better able to capture both the observed relationship between historical emission trajectories and atmospheric CO<sub>2</sub> burden; and the behaviour of ESMs in idealised concentration increase and pulse emission experiments. FaIR v1.0 used four equations to model the atmospheric gas cycle and corresponding effective radiative forcing (ERF) impact of CO<sub>2</sub>, and a further two (unchanged from the AR5-IR) to emulate the climate system's thermal response to changes in ERF. Subsequently, Smith et al. (2018) added a representation of other GHGs and aerosols, which necessarily increased the structural complexity of the model in ~~FaIR-v1~~<sup>v1</sup>FaIRv1.3. In this update, we maintain the ability to simulate the atmospheric response to a wide range of GHGs and aerosol emissions, while attempting to significantly reduce the complexity of the model structure.

In FaIRv2.0.0 we propose a set of six equations that we demonstrate are sufficient to capture the global-mean climate system response to GHG and aerosol emissions. These six equations are outlined in ~~figure~~Figure 1. In this text we explain the physical reasoning behind each equation and select a default parameter set based on simple tunings to historical observations and recent literature. We compare the default response of FaIRv2.0~~to the .0~~ to a publicly available version of the widely used SCM, MAGICC6 (Meinshausen et al., 2011a, b), for a range of Socioeconomic Pathways (Riahi et al., 2017, SSPs). Further, we show that these equations can be tuned to emulate key properties of a range of CMIP6 (Eyring et al., 2016) models. Finally, we constrain a large parameter ensemble inferred from more complex models and contemporary assessments with observations of the present-day warming level and rate to provide a set of observationally constrained probabilistic projections for the future climate following (Smith et al., 2018).

FaIRv2.0.0 is sufficiently simple as to be able to be used in undergraduate and high-school teaching of climate change, and can illustrate some key properties of the climate system such as the warming impacts of different GHGs, the implications of uncertainty in ECS and TCR, or the importance of carbon cycle feedbacks. To allow students and other users unfamiliar with scientific programming languages (such as FaIRv2.0's native language, Python) access to the model, we also provide a version

of FaIRv2.0.0 written in Excel. We hope that this may open exploration of the climate system to a large group of potential users who do not have the expertise to run presently-available SCMs. The simplicity of FaIRv2.0.0 additionally means that although we provide code in a central, open-source repository, which we strongly recommend is used for most cases, users are 90 not forced to rely on this. In fact we expect it would be relatively quick to re-create in whatever language users are familiar with, and in whatever format fits their intended usage.

Here we suggest that the major value of SCMs is in their ability to emulate more complex models, such as has been done in Meinshausen et al. (2011b); Tsutsui (2017, 2020); and in their ability to efficiently integrate massive parameter ensembles 95 for probabilistic climate projection as in Smith et al. (2018); Goodwin et al. (2019). While default parameters must be provided to enable ~~unfamiliar~~ unfamiliar users access to the model, the response arising from these parameters is a function of how they themselves have been selected, rather than one of the model equations themselves. So long as the underlying model equations are sufficiently flexible to emulate a wide range of climate system responses to the variables of interest (for instance the inferred 100 range of responses within the CMIP ensemble), and have a basis in known physical processes, the SCM should be considered to be valid. Although understanding why the default response of SCMs differ is important, comparisons of solely the default response as a test of how “good” a model is are unhelpful; it is likely that any SCM could be re-tuned to better perform against whatever (single) metric is being used for evaluation, whether another SCM, a more complex model, or something else.

In this study we first (~~section 2~~) outline the history and reasoning behind the model equations used in Section 2, including 105 how we selected default parameters, stepping through the concentration response to emissions; the concentration-forcing relationships; and the thermal response to forcing. We then demonstrate how several key components of FaIRv2.0.0 – the carbon cycle, aerosol response and thermal response to forcing – can be tuned to emulate a set of CMIP6 models in ~~section 3~~. Section 3. Section 4 describes the use of FaIRv2.0.0 to constrain climate sensitivities and future surface temperature projections using a large ensemble, following Smith et al. (2018). We then provide a discussion of previous comparisons of SCMs in 110 ~~section~~ Section 5, and suggest some ways in which FaIRv2.0.0 could be used in ~~section~~ Section 6 before concluding.

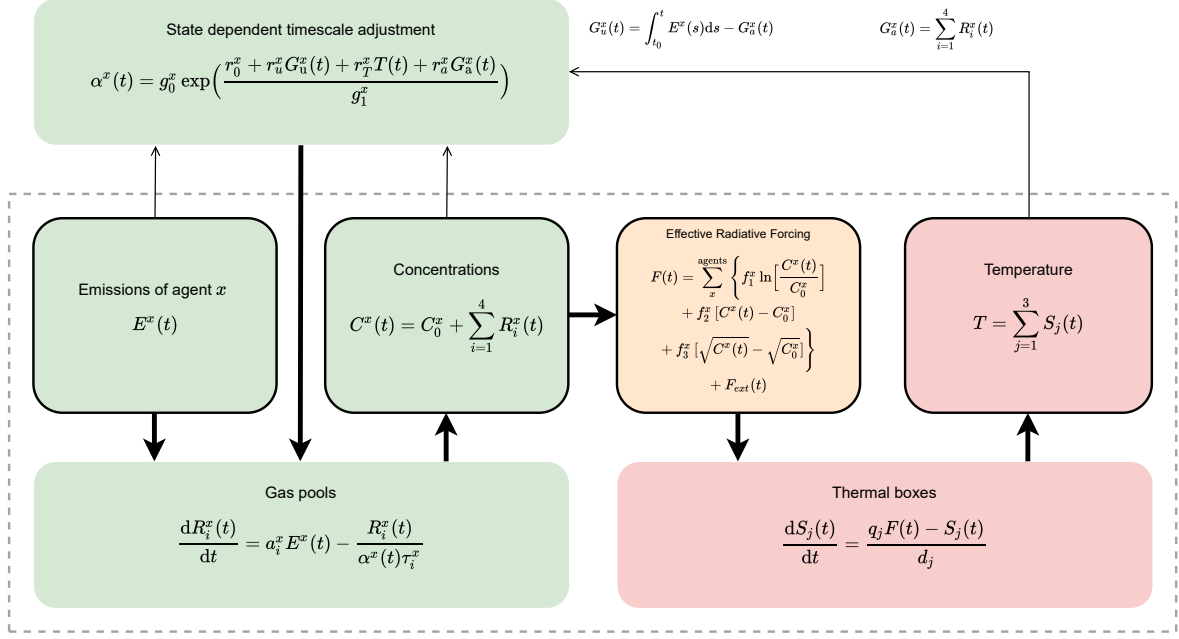


**Figure 1.** Schematic showing the full model structure and equations used. Model steps take place from left to right, with thick arrows indicating Terms without  $(t)$  are constants. Colouring splits the flow of model steps that occur during timestep  $t$  into gas cycle, radiative forcing, and thin arrows indicating steps that occur in between timesteps  $t$  and  $t + dt$ . Equations are described in full below climate response components. The dashed grey line indicates the components identical to AR5-IR (Myhre et al., 2013). Table 1 provides brief descriptions of each named parameter in the figure. We note that under the default parameterisation, for all gases except carbon dioxide, the index  $i$  and associated sums can be removed as these gases are modelled as having a single atmospheric decay timescale only. Equations are described in full in Section 2.1.

parameter units qualitative description  $E(t)$  see table S1 Quantity of agent emitted into atmosphere  $C(t)$  see table S1 Concentration of agent in atmosphere  $C_0$  unit( $C$ ) Pre-industrial concentration of agent in atmosphere  $R_i(t)$  unit( $E$ ) Quantity of agent in  $i^{\text{th}}$  atmospheric pool  $a_i$  Fraction of emissions entering  $i^{\text{th}}$  atmospheric pool  $\tau_i$  yrs Atmospheric lifetime of gas in  $i^{\text{th}}$  pool  $\alpha_i(t)$  Multiplicative adjustment coefficient of pool lifetimes  $r_0$  Strength of pre-industrial uptake from atmosphere  $r_u$  unit( $E$ ) $^{-1}$   
 115 Sensitivity of uptake from atmosphere to cumulative uptake of agent since model initialisation  $r_T$  K $^{-1}$  Sensitivity of uptake from atmosphere to model temperature change since initialisation  $r_a$  unit( $E$ ) $^{-1}$  Sensitivity of uptake from atmosphere to current atmospheric burden of agent  $G_u(t)$  unit( $E$ ) Cumulative uptake of agent since model initialisation  $T$  K Model temperature change since initialisation  $G_a(t)$  unit( $E$ ) Atmospheric burden of agent above pre-industrial levels  $F(t)$  W m $^{-2}$  Effective radiative forcing change since the pre-industrial period  $f_1$  W m $^{-2}$  Logarithmic concentration-forcing coefficient  $f_2$  W m $^{-2}$  unit( $C$ ) $^{-1}$   
 120 Linear concentration-forcing coefficient  $f_3$  W m $^{-2}$  unit( $C$ ) $^{\frac{-1}{2}}$  Square root concentration-forcing coefficient  $S_k(t)$  K Response of  $k^{\text{th}}$  thermal box  $q_k$  K W $^{-1}$  m $^2$  Equilibrium response of  $k^{\text{th}}$  thermal box  $d_k$  yrs Response timescale of  $k^{\text{th}}$  thermal box  $T(t)$  K Surface temperature response since model initialisation

**Table 1.** Qualitative analogies for named parameters in FaIRv2.0.0.

parameter	units	qualitative description
$E(t)$	see table S1	Quantity of agent emitted into atmosphere
$C(t)$	see table S1	Concentration of agent in atmosphere
$C_0$	unit( $C$ )	Pre-industrial concentration of agent in atmosphere
$R_i(t)$	unit( $E$ )	Quantity of agent in $i^{\text{th}}$ atmospheric pool
$a_i$	-	Fraction of emissions entering $i^{\text{th}}$ atmospheric pool
$\tau_i$	yrs	Atmospheric lifetime of gas in $i^{\text{th}}$ pool
$\alpha(t)$	-	Multiplicative adjustment coefficient of pool lifetimes
$r_0$	-	Strength of pre-industrial uptake from atmosphere
$r_u$	unit( $E$ ) $^{-1}$	Sensitivity of uptake from atmosphere to cumulative uptake of agent since model initialisation
$r_T$	K $^{-1}$	Sensitivity of uptake from atmosphere to model temperature change since initialisation
$r_a$	unit( $E$ ) $^{-1}$	Sensitivity of uptake from atmosphere to current atmospheric burden of agent
$G_u(t)$	unit( $E$ )	Cumulative uptake of agent since model initialisation
$T$	K	Model temperature change since initialisation
$G_a(t)$	unit( $E$ )	Atmospheric burden of agent above pre-industrial levels
$F(t)$	W m $^{-2}$	Effective radiative forcing change since the pre-industrial period
$f_1$	W m $^{-2}$	Logarithmic concentration-forcing coefficient
$f_2$	W m $^{-2}$ unit( $C$ ) $^{-1}$	Linear concentration-forcing coefficient
$f_3$	W m $^{-2}$ unit( $C$ ) $^{\frac{-1}{2}}$	Square root concentration-forcing coefficient
$S_j(t)$	K	Response of $j^{\text{th}}$ thermal box
$q_j$	K W $^{-1}$ m $^2$	Equilibrium response of $j^{\text{th}}$ thermal box
$d_j$	yrs	Response timescale of $j^{\text{th}}$ thermal box
$T(t)$	K	Surface temperature response since model initialisation

## 2 FaIRv2.0.0 model framework

As with the previous iteration, FaIRv2.0.0 is a 0D model of globally averaged variables. It models the GHG emission → concentration → effective radiative forcing (ERF), aerosol emission → ERF, and ERF → temperature responses of the climate system. Here we present the equations behind these responses, separating out the model into the key components.

### 2.1 The gas cycle

FaIRv2.0.0 inherits the GHG gas cycle equations directly from the carbon cycle equations within FaIRv1.5 (Smith et al., 2018) and v1.0 (Millar et al., 2017). This carbon cycle adapts the 4-pool-4-timescale impulse-response function model in 125 Joos et al. (2013) for carbon dioxide in Joos et al. (2013) by introducing a state-dependent timescale adjustment factor,  $\alpha$ . This factor scales the decay timescale-timescales of atmospheric carbon into each of the 4 pools, allowing for the effective carbon sink from the atmosphere to change in strength. This allows FaIRv2.0.0 to represent non-linearities in the carbon-cycle in a manner similar to Joos et al. (1996) or Hooss et al. (2001). In Millar et al. (2017) Joos et al. (1996) or Hooss et al. (2001) . In Millar et al. (2017),  $\alpha$  was calculated through a parameterisation of the 100-year integrated Impulse Response Function 130 (iIRF<sub>100</sub>, the average airborne fraction over a period of 100 years). In Millar et al. (2017), the iIRF<sub>100</sub> was parameterised by a simple linear relationship with the quantity of carbon removed since initialisation  $G_u$ , and the current temperature  $T$ :

$$\text{iIRF}_{100} = r_0 + r_u G_u + r_T T,$$

$$\text{iIRF}_{100} = r_0 + r_u G_u + r_T T, \quad (1)$$

140 where  $r_0$  is the initial (pre-industrial) iIRF<sub>100</sub>, and  $r_u$  and  $r_T$  control how the iIRF<sub>100</sub> changes as the cumulative carbon uptake and temperature increases from the atmosphere and temperature change. This parameterisation was informed by the behaviour of ESMs and remains consistent with the key feedbacks involved in the carbon cycle (K. Arora et al., 2020). However, in Millar et al. (2017), the root of a-an implicit non-linear equation had to be found to update  $\alpha$  at each model timestep. The 145 solution of this equation is approximately exponential in iIRF<sub>100</sub> to a high degree of accuracy for a wide range of values, and so in FaIRv2.0.0,  $\alpha$  is calculated using the exponential form given below in equation 4. We parameterise this carbon cycle to enable it to simulate a wide range of GHGs, as discussed below in Section 2.1.1. The equations for the carbon cycle and all other gas cycles are, in their most general form:

$$\frac{dR_i(t)}{dt} = a_i E(t) - \frac{R_i(t)}{\alpha\tau_i} \frac{R_i(t)}{\alpha(t)\tau_i}, \quad (2)$$

150  $C(t) = C_0 + \sum_{i=1}^n R_i(t), \text{ and} \quad (3)$

$$\alpha(t) = g_0 \cdot \exp\left(\frac{r_0 + r_u G_u(t) + r_T T(t) + r_a G_a(t)}{g_1}\right); \quad (4)$$

where  $G_a(t) = \sum_{i=1}^n R_i(t)$ ,

$$G_u(t) = \sum_{s=t_0}^t E(s) - G_a(t);$$

and  $g_1 = \sum_{i=1}^n a_i \tau_i [1 - (1 + 100/\tau_i) e^{-100/\tau_i}]$ ,

and  $g_0 = \exp\left(-\frac{\sum_{i=1}^n a_i \tau_i [1 - e^{-100/\tau_i}]}{g_1}\right)$ .

155

Equations 2 and 3 describe a gas cycle with an atmospheric burden above the pre-industrial concentration,  $C_0$ , formed of  $n$  pools: each pool reservoirs: each reservoir corresponds to a different sink decay timescale from the atmosphere. Each pool These reservoirs do not correspond to any physical carbon stores, but qualitative analogies for them can be found in Millar et al. (2017)

160 . Each reservoir,  $R_i$ , has an uptake fraction  $a_i$  and decay timescale  $\alpha\tau_i$ . At each timestep, the state-dependent adjustment,  $\alpha$ , is computed and the pool reservoir concentrations are updated and aggregated to determine the new atmospheric burden. The new atmospheric concentration is then simply the sum of the burden and the pre-industrial concentration. Here we emphasize that although we have presented this equation set in its general form, with  $n$  reservoirs, in practice we set  $n = 4$  for the carbon-cycle, following Joos et al. (2013); and  $n = 1$  emissions for all other gases within FaIRv2.0.0. For the case where  $n = 1$ , equations 2

165 and 3 can be simplified by dropping the index  $i$  entirely.  $\alpha$  provides feedbacks to the gas lifetimes-lifetime(s) based on the current timestep's levels of accumulated emissions ( $G_u$ ), global temperature ( $T$ ), and atmospheric gas burden ( $G_a$ ).  $G_a$  is included to enable FaIRv2.0.0 to emulate the sensitivity of the CH<sub>4</sub> lifetime to its own atmospheric burden, as predicted by atmospheric chemistry and simulated in chemical transport models (CTMs) (Holmes et al., 2013; Prather et al., 2015). We also find that the emulation of the carbon-cycle of a number of CMIP6 models over the 1pctCO<sub>2</sub> experiment is significantly improved if

170  $G_a$  is included in the iIRF<sub>100</sub> parameterisation; see 3.2. In the default parameterisation of FaIRv2.0.0, this state dependence is only active for carbon dioxide and methane; for all other gases,  $\alpha$  is constant.  $g_0$  and  $g_1$  are constants that set the value and gradient of our analytic approximation for  $\alpha$  equal to the numerical solution of the Millar et al. (2017) iIRF<sub>100</sub> parameterisation at  $\alpha = 1$ , and are therefore determined by the final two equations above and not independent parameters.

175 for the carbon-cycle. An important point is that although we inherit the iIRF timescale of 100 years from Millar et al. (2017) and Joos et al. (2013), this timescale does not affect the behaviour of the model, only the quantitative values of the parameters. Hence for a given emulation target (such as the C4MIP models in Section 3.2) the optimal model fit is independent of the

length of this timescale, but the optimal parameter values are not. Maintaining this timescale at 100 years ensures that the  $r$  coefficients found here are comparable to the previous iterations of FaIR (Smith et al., 2018; Millar et al., 2017). In the following section, we discuss how we parameterise the gas cycle to enable FaIRv2.0.0 to simulate a wide range of GHGs using these  
180 same three equations. Qualitative analogies for each parameter to aid understanding are given in [table](#)-[Table](#) 1.

Here we emphasize the advantage of using this common framework to simulate the response to all the different GHG and aerosol emissions: if a user is able to understand the FaIRv2.0.0 carbon cycle, then they understand how the model will respond to emissions of any other GHG or aerosol. This is because [the carbon cycle](#)-carbon dioxide is the most complex parameterisation  
185 of the above equations([it is the only gas that is simulated](#): being the only species with more than one atmospheric [pool as discussed below](#))decay timescale; and alongside methane one of the only two species to make use of the state-dependence through  $\alpha$  within the default parameterisation. This structural simplicity makes gaining familiarity with the model far easier than if several different gas cycle formulations were used for different GHGs.

### 2.1.1 Parameterising the gas cycle for a wide range of GHGs

190 In this section, we consider how [the above](#)-these equations can be parameterised to represent the gas cycles for many different GHGs. We also provide default parameterisations for each GHG, given in full in [table](#)-[Table](#) S2.

#### Carbon dioxide

As discussed above in [Section 2.1](#), FaIRv2.0.0 retains the state-dependent formulation (Millar et al., 2017) of the [4-pool](#)-[4-timescale](#) impulse-reponse model from [Joos et al. \(2013\)](#)[Joos et al. \(2013\)](#); hence  $n = 4$ . We retain the same state-dependency  
195 as in [Millar et al. \(2017\)](#)[Millar et al. \(2017\)](#), so the  $r$  parameters are non-zero with the exception of  $r_a$ . The [multi-model mean](#)  
[default](#)  $a$  and  $\tau$  coefficients [from Joos et al. \(2013\)](#)[are used by default](#)are the multi-model mean from Joos et al. (2013). Default  
 $r_u$  and  $r_T$  parameters are taken as the mean of the parameter distributions inferred from CMIP6 models in [section](#)-[Section](#)  
200 4.2.1. Following [Jenkins et al. \(2018\)](#)[Jenkins et al. \(2018\)](#), we tune the default  $r_0$  parameter such that present-day (2018) cumulative CO<sub>2</sub> emissions match the [Global Carbon Project \(GCP\) estimates](#) ([Friedlingstein et al., 2019](#))RCMIP emission protocol  
[\(Nicholls et al., 2020a\)](#) when historical concentrations (Meinshausen et al., 2017) are inverted back to emissions by equations  
2, 3 and 4. Here we take the [GCP dataset as a best-estimate](#)RCMIP protocol as one estimate of observed emissions, but it is im-  
portant to note that using a different dataset (such as the [RCMIP protocol emissions, which are designed to match the data used](#)  
in [CMIP6 esm runs](#))Global Carbon Project (Friedlingstein et al., 2019), would result in a different value. The pre-industrial  
concentration is fixed at 278 ppm.

#### 205 Methane

We parameterise methane using a single atmospheric sink:  $n = 1$ . Although several individual mechanisms have been identified for the removal of atmospheric methane – tropospheric OH, tropospheric Cl, stratospheric reactions and soil uptake (Prather

et al., 2012; Holmes et al., 2013) – these can be aggregated into a single effective atmospheric lifetime. Through  $r_T$  and  $r_a$ , we include the key lifetime feedback dependence on to its own atmospheric burden, and tropospheric air temperature and water vapour mixing ratio (Holmes et al., 2013). We tune  $r_a$  to match the sensitivity of the methane lifetime to its own atmospheric burden at the present-day found by Holmes et al. (2013).  $r_T$  is tuned to match the sensitivity of the methane lifetime to tropospheric air temperature and water vapour at the present-day found by Holmes et al. (2013). Since both tropospheric air temperature and water vapour are closely related to surface air temperatures (they are often approximated by simple parameterisations of the surface air temperature, as in Holmes et al. (2013)), including these two sensitivities through a single surface temperature feedback closely replicates lifetime behaviour if both are included separately. See Figure S2 for the evolution of the methane lifetime within default FaIRv2.0.0 over history and a future RCP8.5 pathway (Riahi et al., 2011).  $\tau$  is then set such that the mean emission rate since 2000 matches current estimates from the RCMIP database protocol (Nicholls et al., 2020a) when historical concentrations (Meinshausen et al., 2017) are inverted by FaIRv2.0.0; and  $r_0$  is set such that  $\alpha = 1$  at model initialisation. The pre-industrial concentration is fixed at 720 ppm ppb.

## 220 Nitrous oxide

Nitrous oxide is parameterised with a single atmospheric sink, and no lifetime sensitivities:  $n = 1$  and  $\{r_u, r_T, r_a\} = 0$ . Although there is evidence that nitrous oxide has a small sensitivity to its atmospheric burden (Prather et al., 2015), when included in FaIRv2.0.0 this made very little difference to nitrous oxide concentrations, even under high emission scenarios. We therefore do not include this additional complexity.  $\tau$  is set tuned to match the best-estimate present-day residence 225 lifetime in Prather et al. (2015) of 109 years cumulative RCMIP protocol emissions when historical concentrations are inverted by FaIRv2.0.0; and  $r_0$  is set such that  $\alpha = 1$  at model initialisation. The pre-industrial concentration is fixed at 270 ppm.

## Halogenated gases

All other GHGs are treated as having a single atmospheric lifetime and no feedbacks:  $n = 1$  and  $\{r_u, r_T, r_a\} = 0$ . We take lifetime estimates from WMO (2018). Pre-industrial concentrations (if non-zero) are set to the 1750 value from Meinshausen 230 et al. (2017). Inclusion of a temperature-dependent lifetime to represent changes to the Brewer-Dobson circulation (Butchart and Scaife, 2001), as in the MAGICC SCM (Meinshausen et al., 2011a), would be possible through a non-zero  $r_T$  parameter. We do not include a representation of this effect in our default parameters parameterisation due to its small impact on model output and increase in model complexity.

## Aerosols

235 Aerosols have considerably shorter lifetimes than the timescales generally considered by SCMs (Kristiansen et al., 2016). In FaIRv2.0.0, as in previous iterations (Smith et al., 2018) and other SCMs (Meinshausen et al., 2011a), they are therefore converted directly from emissions to radiative forcing. In FaIRv2.0.0, this can be achieved by setting  $n = 1$ ,  $\tau = 1$ , and providing a unit conversion factor of 1 between emissions and “concentrations”.

### 2.1.2 Historical and SSP concentration trajectories

240 Here we compare the default parameterisation gas cycle model in FaIRv2.0.0-alpha to a previous version, FaIRv1.5 (Smith et al., 2018), and to MAGICC7.1.0-beta (Meinshausen et al., 2019), highlighting any differences. All three models are run under the fully emission-driven “esm-allGHG” RCMIP protocol (Nicholls et al., 2020a); ~~in the case of FaIRv2.0 we use data from the Global Carbon Project (Friedlingstein et al., 2019) for the input CO<sub>2</sub> emissions.~~ FaIRv2.0.0 matches trajectories from both its previous iteration and the more comprehensive MAGICC closely for all GHGs. We note some discrepancies in the  
245 timeseries for halogenated gases between FaIRv2.0.0 and MAGICC, possibly due to the incorporation of a state-dependent OH abundance and representation of changes to the Brewer-Dobson circulation which modulate the lifetimes of these gases (Meinshausen et al., 2011a). We note that for these gases we could have matched historical concentrations closer by tuning the lifetimes to the RCMIP ~~emission protocol data~~ and historical concentration timeseries (Nicholls et al., 2020a; Meinshausen et al., 2017), but argue that taking the best-estimate lifetimes from WMO (2018) is defensible; it is more transparent and  
250 avoids ~~emission source dependent~~ source-dependent parameters (if a different emission dataset were used, the resulting tuned lifetimes would be different). The lower CO<sub>2</sub> concentration projections in FaIRv2.0.0 compared to FaIRv1.5 are due to weaker temperature and cumulative carbon uptake feedbacks (lower  $r_u$  and  $r_T$ ) as inferred from the CMIP6 carbon cycle tunings performed in ~~section 3.2~~. Section 3.2.

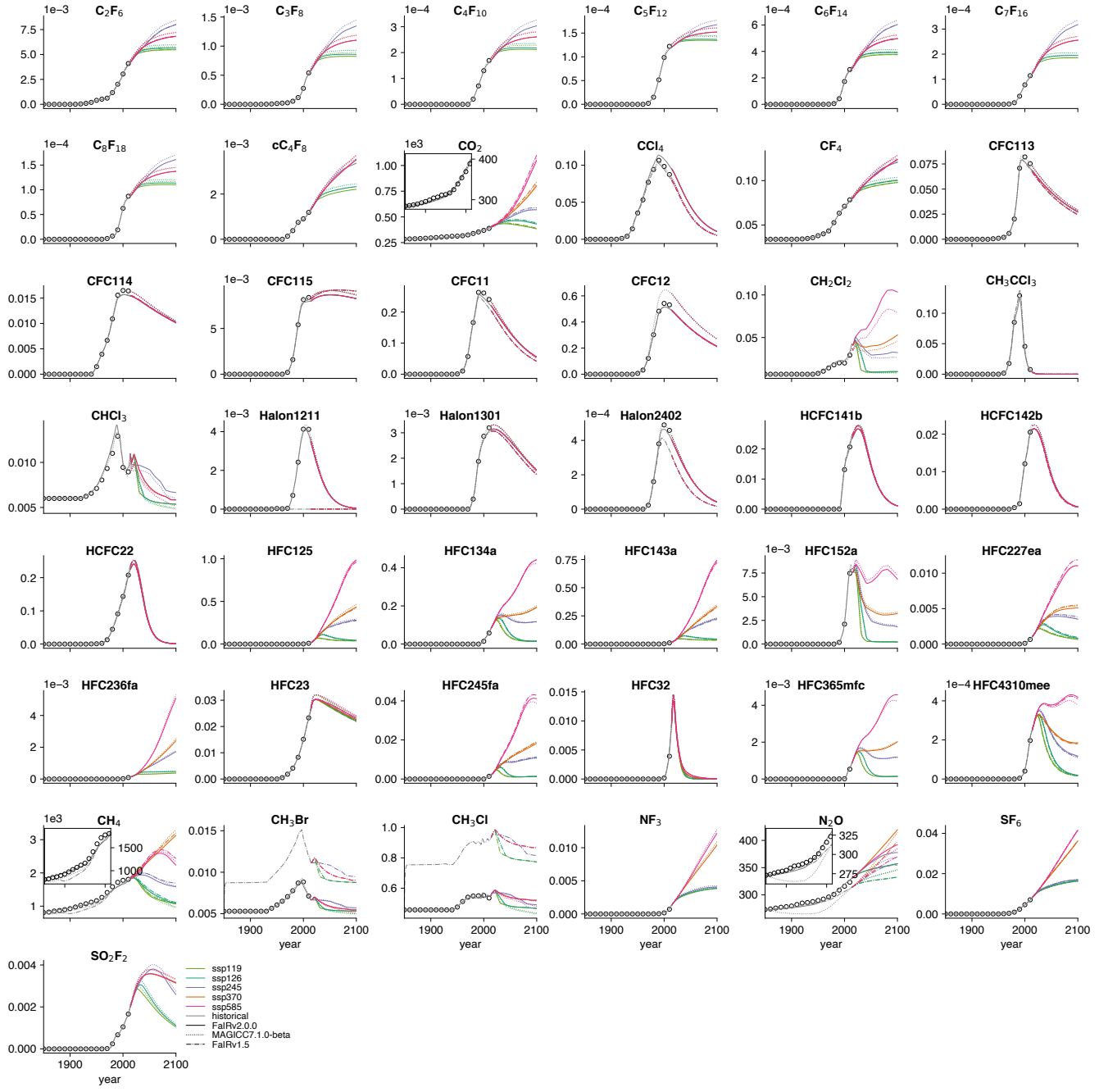


**Figure 2.** Comparison of historical and future concentration trajectories over a range of SSPs. Units for all GHGs are ppb with the exception of  $\text{CO}_2$  which is plotted in ppm. Inset panels for  $\text{CH}_4$ ,  $\text{N}_2\text{O}$ , and  $\text{CH}_3\text{Cl}$  show the historic period.

## Specification of natural emissions

255 In FaIRv2.0.0 we have chosen to formulate the gas cycle equations in terms of a perturbation above the pre-industrial (natural equilibrium) concentration. By definition, this assumes a time-independent quantity of natural emissions for each gas (which can be derived from the pre-industrial concentration and lifetime of the gas). This differs from Meinshausen et al. (2011a) and Smith et al. (2018), who (when driving the respective models with emissions and with the exception of CO<sub>2</sub>) require a quantity of natural emissions to be supplied in addition to any anthropogenic emissions by default (though the models can also be run in  
 260 a fully emission-driven mode as in [figure](#)[Figure](#) 2). Over the historical period, these emissions are chosen such that they “close the budget” between total anthropogenic emissions, and observed concentrations (Meinshausen et al., 2011a; Smith et al., 2018). This procedure of balancing the budget over history is analogous to driving the model with concentrations up to the present day, and then switching to driving the model with emissions afterwards. While this methodology has the advantage of ensuring the model simulates present-day concentrations that match observation exactly, it loses consistency between the way in  
 265 which the model simulates the past and the future. If care is not taken when running these models, this loss of consistency could lead to discontinuities at the present-day (when the model switches from concentration- to emission-driven). As present-day trends are crucial for the estimation of many policy and scientifically relevant quantities such as TCR, TCRE and remaining carbon budgets (Leach et al., 2018; Tokarska et al., 2020; Jiménez-de-la Cuesta and Mauritsen, 2019), we have chosen to enforce a consistent model (ie. emission- *or* concentration-driven) over the entire simulation period in FaIRv2.0.0. We note  
 270 that replicating this budget closing procedure is possible in FaIRv2.0.0 by inverting observed concentrations to emissions and then joining these inverse emission timeseries to any future scenarios manually. In this study, FaIRv2.0.0 is run in emission-driven mode unless stated otherwise.

## 2.2 Effective radiative forcing

275 FaIRv2.0.0 uses a simple formula to relate atmospheric gas concentrations to effective radiative forcing. This equation, [below](#)5, includes logarithmic, square-root, and linear terms; motivated by the concentration-forcing relationships in Myhre et al. (2013) of CO<sub>2</sub>, CH<sub>4</sub> and N<sub>2</sub>O, and all other well-mixed GHGs respectively. For most agents, the concentration- (or for aerosols, emission-) forcing relationship can be reasonably approximated by one of these terms in isolation, however if there is substantial evidence the relationship deviates significantly from any one term, others are able to be included to provide a more accurate fit.  $F_{ext}$  is the sum of all exogenous forcings supplied. These may include natural forcing agents or forcing due to  
 280 albedo changes.

$$F(t) = \sum_x^{\text{forcing agents}} \left\{ f_1^x \cdot \ln \left[ \frac{C^x(t)}{C_0^x} \right] + f_2^x \cdot [C^x(t) - C_0^x] + f_3^x \cdot [\sqrt{C^x(t)} - \sqrt{C_0^x}] \right\} + F_{ext}. \quad (5)$$

## 2.2.1 Parameterising the forcing equation

### Carbon dioxide, nitrous oxide and methane

We assume the forcing relationship for carbon dioxide is well approximated by the combination of a logarithmic and square root term (Ramaswamy et al., 2001),  $f_2^{CO_2} = 0$ ; both the methane and nitrous oxide concentration-forcing relationships are approximated by a square root term only,  $f_{1,2}^{CH_4, N_2O} = 0$ . Although overlaps between the spectral bands of these gases mean more complex function forms including interaction terms represent our current best approximation to the observed relationship from spectral calculation (Etminan et al., 2016), inclusion of these interaction terms significantly increases the structural complexity of the model. These overlap terms are most significant for very high concentrations of these gases, and we find that the more simple relationships used here are sufficiently accurate within the context of the uncertainties associated with such high concentration scenarios. We fit the non-zero  $f$  coefficients to the Oslo-line-by-line (OLBL) data from Etminan et al. (2016). Our resulting fits have a maximum absolute error of  $0.115 \text{ W m}^{-2}$  when compared to the OLBL data, though this is for the most extreme-high concentration data point; and the associated relative error is 1.1%. Figure S1 provides a complete comparison of how the fit relationships used here compare to the OLBL data, and to the simple formulae which include interaction terms in Etminan et al. (2016).

### Halogenated GHGs

Following other simple models (Smith et al., 2018; Meinshausen et al., 2011a), we assume concentrations of halogenated gases are linearly related to their direct effective radiative forcing,  $f_{1,3}^x = 0$ . The conversion coefficient for each gas is its radiative efficiency, which we take from WMO (2018).

## 300 Aerosol-radiation interaction

We follow Smith et al. (2020), parameterising the ERF due to aerosol radiation interaction as a linear function of sulphate, organic carbon and black carbon aerosol emissions:

$$\text{ERFari} = f_2^{SO_2} E^{SO_2} + f_2^{OC} E^{OC} + f_2^{BC} E^{BC}. \quad (6)$$

Default parameters are taken as the ~~mean of parameters tuned to 10 CMIP6 models in (Smith et al., 2020, see section 3.3)~~  
305 ~~central estimate from the CONSTRAINED ensemble described in Section 4.~~

### Aerosol-cloud interaction

ERF due to aerosol-cloud interactions is parameterised following a modification of Smith et al. (2020), as a logarithmic function of sulphate aerosol emissions, and a linear function of organic carbon and black carbon aerosol emissions:

$$\text{ERFaci} = f_1^{aci} \ln \left( 1 + \frac{E_{SO_2}}{C_0^{SO_2}} \right) + f_2^{aci} (E^{OC} + E^{BC}). \quad (7)$$

310 Here  $C_0^{SO_2}$  effectively acts as a shape parameter for the logarithmic term. We fit this functional form to the ERFaci component in 10 CMIP6 models derived by the Approximate Partial Radiative Perturbation method (Zelinka et al., 2014) in section 3.3. The default value for the OC+BC coefficient is taken as the mean of the CMIP6 fits. For the logarithmic coefficient and shape parameter, which appear to have highly skewed distributions due to some models displaying linear and others displaying logarithmic behaviour against sulphate emissions, we calculate default parameters as the mean of the CMIP6 fits, assuming the underlying distribution is lognormally distributed. Section 3.3. Default parameters are taken as the central estimate from the CONSTRAINED ensemble described in Section 4.

### Tropospheric ozone

320 Tropospheric ozone is parameterised following (Stevenson et al., 2013) Thornhill et al. (2021), as a linear function of methane, nitrous oxide and ODS concentrations, and nitrate aerosol, carbon monoxide, and volatile organic compound emissions. For the methane component, default coefficients are taken from Holmes et al. (2013). For the others, default coefficients are found by dividing the attributed forcing in (Myhre et al., 2013) by the 2011 emission rate from the Community Emissions Data System (CEDS) inventory (Hoesly et al., 2018).

### Stratospheric ozone

325 Stratospheric ozone ERF is parameterised as a linear function of the concentration of ozone-depleting substances (ODSs). We assume that the cumulative ERF of a gas over its lifetime is proportional to its ozone depletion potential (WMO, 2018). The best-estimate AR5 value for stratospheric ozone ERF of  $0.05 \text{ W m}^{-2}$  and observed concentrations of each ODS (Meinshausen et al., 2017) in 2011 then allows us to calculate default linear coefficients for each gas. This parameterisation is tuned such that the overall ozone forcing timeseries re-produces Skeie et al. (2020). The contribution of individual ODSs to their total is based on their estimated equivalent effective stratospheric chlorine (Newman et al., 2007; Velders and Daniel, 2014; Smith et al., 330 , with fractional release factors from Engel et al. (2018)).

### Stratospheric water vapour

Stratospheric water vapour is assumed to be a linear function of methane concentrations (Smith et al., 2018) due to its small magnitude. The default coefficient is derived from the indirect forcing components in Holmes et al. (2013):  $5.5 \times 10^{-5}$  5<sup>th</sup> Assessment Report forcing estimate (Myhre et al., 2013) and historical methane concentrations (Meinshausen et al., 2017): 335  $4.37 \times 10^{-5} \text{ W m}^{-2} \text{ ppb}^{-1}$ .

### Black carbon on snow

ERF due to light absorbing particles on snow and ice remains a linear function of black carbon emissions (Smith et al., 2018). In AR5, the best estimate of its associated ERF was  $0.04 \text{ W m}^{-2}$  (Myhre et al., 2013). However, this value is very uncertain, and the efficacy of black carbon on snow may at least double this value (Bond et al., 2013). We therefore calculate our default

340 forcing efficiency by dividing an adopted value of  $-0.08 \text{ W m}^{-2}$  by the **CEDS RCMIP protocol** emission rate:  $0.011\text{--}0.0116 \text{ W m}^{-2} \text{ MtBC}^{-1}$ .

## Contrails

Combined ERF due to contrails and contrail-induced cirrus is modelled as a linear function of aviation-sector  $\text{NO}_x$  emissions. The default coefficient is calculated by dividing the best-estimate present-day contrail ERF (Lee et al., 2021) by the **CEDS RCMIP protocol** emission rate:  $0.011\text{--}0.0164 \text{ W m}^{-2} \text{ MtNO}_x^{-1}$ .

## Albedo shift due to land-use change

In this study we prescribe ERF due to land-use change externally. However, it could be incorporated in a manner identical to FaIRv1.5 by supplying a time-series of cumulative land-use change  $\text{CO}_2$  emissions, and scaling linearly by a coefficient of  $-0.00114 \text{ W m}^{-2} \text{ GtC}^{-1}$  (Smith et al., 2018).

350 **2.3 Default parameter metric values for comparison**

Table S3 contains default parameter calculated values for the global warming potential (Lashof and Ahuja, 1990) of each emission type simulated in FaIRv2.0.0. These values are intended to aid comparison between FaIRv2.0.0 and other SCMs and do not represent any new analysis.

## 2.4 Temperature response

355 The final component of the model calculates the surface temperature response to the changes in ERF. A common representation of this physical process is the energy balance model outlined by Geoffroy et al. (2013). Here we consider the three-box energy balance model, including the ocean heat uptake efficacy factor introduced by Held et al. (2010). Recent literature has suggested that a two-box energy balance model is insufficient to capture the full range of behaviour observed in CMIP6 models (Tsutsui, 2020, 2017; Cummins et al., 2020). The three-box model can be written in state-space form as:

360

$$\begin{aligned} \dot{\mathbf{X}}(t) &= A\mathbf{X}(t) + \mathbf{b}F(t), \\ \underline{\mathbf{Y}} = \underline{C_d}\mathbf{X}; \text{where } \mathbf{X}(t) &= \begin{pmatrix} T_1(t) & T_2(t) & T_3(t) \end{pmatrix}^T, \\ A &= \begin{pmatrix} -(\lambda + \kappa_2)/C_1 & \kappa_2/C_1 & 0 \\ \kappa_2/C_2 & -(\kappa_2 + \epsilon\kappa_3)/C_2 & \epsilon\kappa_3/C_2 \\ 0 & \kappa_3/C_3 & -\kappa_3/C_3 \end{pmatrix}, \\ \underline{\mathbf{Y}} \text{ and } \mathbf{b} &= \underline{1} \begin{pmatrix} 1/C_1 & 0 & 0 \end{pmatrix}^T \text{ and } \underline{C_d} = . \end{aligned} \quad (8)$$

365

Here, each box  $i$  has a temperature  $T_i$  and heat capacity  $C_i$ .  $F$  is the prescribed radiative forcing and  $N$  is the observed

**top-of-atmosphere energy imbalance.** Heat exchange coefficients  $\kappa$  represent the strength of thermal coupling between boxes  $i$  and  $i - 1$ .  $\lambda$  is the so-called climate feedback parameter.  $\epsilon$  is the efficacy factor that enables the energy balance model to account for the variations in  $\lambda$  during periods of transient warming observed in GCMs.  $T_1$  represents the surface temperature change relative to a pre-industrial climate. For many users of SCMs, the key variable of interest is  $T_1$ , the surface temperature response. **Calculating** To allow parameters of this energy-balance model to be fit to finite-length CMIP6 experiments with any degree of certainty, Cummins et al. also take advantage of the following relationship with the top of atmosphere flux,  $N(t)$ :

$$N(t) = F(t) - \lambda T_1(t) + (1 - \epsilon) \kappa_3 [T_2(t) - T_3(t)] \quad (9)$$

375

However, calculating the surface temperature response to radiative forcing within the energy-balance model can be simplified by diagonalising equation 8, resulting in an impulse-response in  $T_1$  (henceforth referred to as  $T$ ), giving the thermal response form in Millar et al. (2017) (Tsutsui, 2017):

$$380 \quad \frac{dS_j(t)}{dt} = \frac{q_j F(t) - S_j(t)}{d_j} \quad (10)$$

$$\text{and } T(t) = \sum_{j=1}^3 S_j(t). \quad (11)$$

The response timescales,  $d_i$ , are given by  $\frac{-1}{e_i}$ , where  $e_i$  are

We can relate the energy-balance model matrix representation to the impulse-response parameters as follows. If we let  $\Phi$  be the matrix that diagonalises  $A$  such that  $\Phi^{-1} A \Phi = D$ , where  $D$  is a diagonal matrix with the eigenvalues of  $A_{ij; 2 \leq i,j \leq 4}$ , and 385 the response coefficients,  $q_i$ , are given by the product of  $e_i$  with the first element of the associated right and left eigenvectors of  $A_{ij; 2 \leq i,j \leq 4}$  on the diagonals, then the response timescales are  $d_i = -1/D_{ii}$  (Geoffroy et al., 2013). The response coefficients are  $q_i = d_i \Phi_{i,0}^{-1} \Phi_{0,i} / C_1$ . In FaIRv2.0.0, we use this three timescale impulse response form due to its simplicity and flexibility. Two common measures of the climate sensitivity, the equilibrium climate sensitivity (ECS) and transient climate response (TCR) (Collins et al., 2013) are easily expressed in terms of the impulse response parameters:

390

$$\text{ECS} = F_{2 \times \text{CO}_2} \cdot \sum_{i=1, j=1}^3 q_{ij} \quad (12)$$

$$\text{TCR} = F_{2 \times \text{CO}_2} \cdot \sum_{i=1, j=1}^3 \left\{ q_{ij} \left( 1 - \frac{d_i}{70} \frac{d_j}{70} \left[ 1 - e^{-\frac{70}{d_i} - \frac{70}{d_j}} \right] \right) \right\}. \quad (13)$$

The default thermal response parameters in FaIRv2.0.0 are derived as follows.  $d_1, d_2, d_3$  and  $q_1$   $d_1 = 0.903$ ,  $d_2 = 7.92$ ,  $d_3 = 355$  and  $q_1 = 0.180$  are taken as the central value of their central value within the CONSTRAINED ensemble in Section 4.3, which do not differ significantly from the CMIP6 inferred distributions described in section 4.2.3.  $q_2$  and  $q_3$  distribution

described in Section 4.2.3.  $q_2 = 0.297$  and  $q_3 = 0.386$  are then set by equations 12 and 13 such that the default parameter set response has climate sensitivities (ECS and TCR) equal to the central values of the constrained ensemble described in section 4: ECS = 3.2–3.24 K and TCR = 1.8–1.79 K.

## 400 3 Emulating complex climate models

In this section we demonstrate the ability of FaIRv2.0.0 to emulate the more complex models from CMIP6 (Eyring et al., 2016) in a limited set of experiments. Due to constraints on data availability, we have focussed on tuning the key components of the model: the carbon cycle; the thermal response; and the aerosol ERF relationships. We use the abrupt-4xCO<sub>2</sub> and 1pctCO<sub>2</sub> CMIP6 experiments to tune the carbon cycle and thermal response. The highly idealised nature of these experiments means 405 that parameters arising from these tunings will not necessarily be able to emulate complex model response to more realistic scenarios due to processes that FaIRv2.0.0 cannot represent. In the near future we hope to be able to tune to the historical and SSP CMIP6 experiments in order to validate the tunings given here.

### 3.1 Tuning the thermal response

We follow the statistically rigorous methodology of Cummins et al. (2020) to tune thermal response parameters to 40–28 410 CMIP6 models. This involves fitting parameters to the energy balance model ~~above outlined in equation 8~~ by recursively computing the likelihood via ~~the-a~~ Kalman filter; the optimal parameters are those that maximise the computed likelihood. We then transform the ~~calculated~~ optimal energy balance parameters into the impulse response form used in FaIRv2.0.0. We obtain model data from the “abrupt-4xCO<sub>2</sub>”, “1pctCO<sub>2</sub>” and “piControl” experiments for the top-of-energy imbalance and 415 surface temperature response from ESGF (Cinquini et al., 2014). ~~We calculate anomalies and correct for model drift in the abrupt-4xCO<sub>2</sub> and 1pctCO<sub>2</sub> experiments using output from the piControl experiment, based on the CMOR parent branch time metadata~~ These data are normalised as described in Nicholls et al. (2021). To reduce ~~noise~~ internal variability in the input ~~datatimeseries used to fit parameters~~, we average over all available ensemble members for each model. ~~For full details of this anomaly-correction procedure, see the supplement~~ The number of ensemble members per model is stated in Table S4. The Cummins et al. (2020) methodology uses surface temperatures and top-of-atmosphere energy imbalances (as related by 420 equation 9) from the abrupt-4xCO<sub>2</sub> experiment to return all the parameters of the energy balance model ~~above~~, plus the radiative forcing arising from the quadrupling of carbon dioxide concentrations. While this would fully specify both the thermal response and the concentration-forcing relationship if concentration-forcing was a pure logarithmic relationship, several models display significant deviations from a pure logarithmic concentration-forcing relationship (Tsutsui, 2020, 2017). We account for this 425 within the FaIR-FaIRv2.0.0 framework by assuming that the concentration-forcing relationship can be reasonably approximated by the sum of a logarithmic and square-root term. Best-estimate  $f_1^{CO_2}$  and  $f_3^{CO_2}$  parameters are found by first deriving the TCR of each model using the 1pctCO<sub>2</sub> experiment. We can use the tuned impulse-response parameters and TCR to then calculate the forcing at a doubling of carbon dioxide using the relationship ~~above~~ in equation 13. The forcings at carbon dioxide doubling and quadrupling uniquely specify  $f_1^{CO_2}$  and  $f_3^{CO_2}$  values for use in FaIR-FaIRv2.0.0. The best-estimate impulse-

response and  $f$  parameters, climate sensitivities, and forcings at carbon dioxide doubling and quadrupling are given [below](#) in

430 [Table 2](#). Corresponding energy balance model parameters are given in [the supplement](#)[Table S5](#). Figure 3 shows the emulated and original responses to the abrupt-4xCO<sub>2</sub> and 1pctCO<sub>2</sub> experiments for each model.

**Table 2.** Tuned CMIP6 thermal response parameters.

model	$d_1$	$d_2$	$d_3$	$q_1$	$q_2$	$q_3$	$F_{\text{ECS}}$	$\text{TCR}$	$\text{CM2}$	$\text{ACCESS-CM2}$	$0.8140$	$8.980$	$339.0$	$0.168000$	$0.508$	$0.810000$				
	$3.18$	$7.20$	$4.72$	$2.18$	$\text{ACCESS-ESM1-5}$	$0.6380$	$6.010$	$342.0$	$0.119000$	$0.447$	$0.865000$	$3.53$	$6.55$	$5.05$	$2.15$	$\text{AWI-CM-1-1-MR}$	$1.1600$	$6.950$		
	$170.0$	$0.222000$	$0.296$	$0.337000$	$3.96$	$7.85$	$3.39$	$2.16$	$\text{BCC-CSM2-MR}$	$1.2200$	$7.230$	$225.0$	$0.176000$	$0.341$	$0.566000$	$3.28$	$6.16$	$3.55$	$1.83$	
	$\text{BCC-ESM1-2}$	$0.1000$	$9.880$	$282.0$	$0.289000$	$0.305$	$0.539000$	$3.18$	$6.25$	$3.60$	$1.92$	$\text{CAMS-CSM1-0}$	$0.03360$	$4.230$	$132.0$	$0.072500$	$0.297$			
	$0.166000$	$4.61$	$8.74$	$2.47$	$1.79$	$\text{CESM2-4.1}$	$1300$	$81.700$	$929.0$	$0.0676000$	$0.644$	$1.120000$	$2.58$	$5.52$	$6.28$	$2.28$	$\text{CESM2-FV2}$	$0.5670$	$4.600$	$427.0$
	$0.093900$	$0.448$	$1.280000$	$3.35$	$7.39$	$6.09$	$2.04$	$\text{CESM2-WACCM}$	$0.3180$	$4.740$	$330.0$	$0.052700$	$0.470$	$0.872000$	$3.71$	$8.06$	$5.17$	$2.14$		
	$\text{CESM2-WACCM-FV2}$	$0.6350$	$6.220$	$469.0$	$0.0140000$	$0.461$	$1.190000$	$2.99$	$6.74$	$5.34$	$1.92$	$\text{CNRM-CM6-1}$	$1.1600$	$7.600$	$242.0$	$0.152000$	$0.424$			
	$0.867000$	$3.91$	$8.38$	$5.64$	$2.51$	$\text{CNRM-CM6-1-1}$	$1.5900$	$25.700$	$1160.0$	$0.0352000$	$0.401$	$0.045400$	$3.25$	$8.74$	$2.59$	$1.98$	$\text{CNRM-CM6-1-HR}$	$1.1700$	$11.600$	$233.0$
	$0.235000$	$0.454$	$0.293000$	$3.92$	$7.94$	$3.85$	$2.55$	$\text{CNRM-ESM2-1}$	$1.17300$	$11.200$	$367.0$	$0.0280000$	$0.542$	$0.683000$	$2.59$					
	$6.01$	$3.90$	$2.04$	$\text{CanESM5}$	$1.1600$	$11.300$	$296.0$	$0.0232000$	$0.571$	$0.770000$	$3.43$	$7.42$	$5.39$	$2.71$	$\text{E3SM-1-0}$	$0.9690$	$11.300$	$275.0$	$0.0203000$	
	$0.698$	$0.832000$	$3.52$	$7.00$	$6.10$	$3.10$	$\text{EC-Earth3-Veg}$	$0.8550$	$7.570$	$119.0$	$0.0201000$	$0.400$	$0.587000$	$3.59$	$7.47$	$4.27$	$2.51$	$\text{GFDL-CM4}$	$0.0298$	
	$2.370$	$253.0$	$0.000024$	$0.427$	$0.558000$	$4.20$	$8.95$	$4.14$	$2.03$	$\text{GFDL-ESM4}$	$1.1300$	$7.890$	$292.0$	$0.0227000$	$0.253$	$0.154000$	$3.39$	$7.87$	$2.15$	$1.58$
	$\text{GISS-E2-1-G}$	$0.9460$	$5.610$	$369.0$	$0.0202000$	$0.226$	$0.233000$	$4.28$	$8.14$	$2.83$	$1.83$	$\text{GISS-E2-1-H}$	$1.5400$	$35.500$	$1.11e8$	$0.318000$	$0.278$			
	$0.000075$	$4.61$	$8.38$	$2.75$	$2.15$	$\text{GISS-E2-2-G}$	$0.8250$	$9.900$	$896.0$	$0.0209000$	$0.235$	$0.038500$	$4.04$	$8.20$	$1.95$	$1.65$	$\text{HadGEM3-GC31-LL}$	$0.8600$		
	$9.310$	$279.0$	$0.0167000$	$0.604$	$0.863000$	$3.30$	$7.22$	$5.39$	$2.60$	$\text{HadGEM3-GC31-MM}$	$1.1200$	$12.300$	$237.0$	$0.0276000$	$0.477$	$0.762000$	$3.36$	$7.20$		
	$5.10$	$2.58$	$\text{INM-CM4-8}$	$1.0700$	$6.190$	$79.3$	$0.207000$	$0.224$	$0.201000$	$2.83$	$5.93$	$1.79$	$1.35$	$\text{INM-CM5-0-1}$	$1.1300$	$7.330$	$165.0$	$0.0217000$	$0.235$	
	$0.185000$	$2.92$	$6.29$	$1.86$	$1.33$	$\text{IPSL-CM6A-LR}$	$1.0600$	$13.500$	$366.0$	$0.0316000$	$0.504$	$0.634000$	$3.06$	$6.98$	$4.46$	$2.38$	$\text{KACE-1-0-G}$	$0.0318$		
	$6.260$	$345.0$	$0.0299000$	$0.480$	$0.867000$	$3.68$	$7.11$	$5.07$	$2.02$	$\text{MIROC-ES2L}$	$3.5700$	$19.400$	$552.0$	$0.0324000$	$0.168$	$0.113000$	$3.84$	$7.89$	$2.33$	
	$1.68$	$\text{MIROC6-1-1000}$	$8.470$	$440.0$	$0.268000$	$0.178$	$0.246000$	$3.56$	$7.80$	$2.46$	$1.56$	$\text{MPI-ESM1-2-HR}$	$1.7200$	$9.630$	$254.0$	$0.0298000$	$0.167$			
	$0.378000$	$3.52$	$7.82$	$2.97$	$1.70$	$\text{MPI-ESM1-2-LR}$	$2.4600$	$72.700$	$6.72e6$	$0.375000$	$0.172$	$0.032000$	$4.19$	$9.48$	$2.43$	$1.77$	$\text{MRI-ESM2-0-1-1100}$	$5.280$		
	$247.0$	$0.0163000$	$0.286$	$0.444000$	$3.48$	$7.47$	$3.11$	$1.68$	$\text{NESM3}$	$1.2400$	$22.900$	$445.0$	$0.0472000$	$0.345$	$0.267000$	$3.75$	$7.86$	$4.06$	$2.70$	
	$\text{NorCPM1}$	$2.5000$	$42.500$	$1.77e8$	$0.334000$	$0.246$	$0.065500$	$3.60$	$7.82$	$2.33$	$1.61$	$\text{NorESM2-LM}$	$0.2310$	$0.938$	$1350.0$	$0.000073$	$0.250$			
	$1.080000$	$5.47$	$11.70$	$7.30$	$1.50$	$\text{NorESM2-MM}$	$0.4290$	$1.210$	$302.0$	$0.000088$	$0.292$	$0.217000$	$4.19$	$10.80$	$2.13$	$1.30$	$\text{SAM0-UNICON}$	$0.8180$		
	$4.580$	$308.0$	$0.0105000$	$0.405$	$0.459000$	$4.57$	$8.33$	$4.43$	$2.42$	$\text{TaiESM1-1-1600}$										
	<b>6.750</b>	<b>274.0</b>	<b>0.0152000</b>	<b>0.428</b>	<b>0.553000</b>	<b>4.07</b>	<b>8.15</b>	<b>4.61</b>	<b>2.45</b>	<b>UKESM1-0-LL</b>	<b>0.7530</b>	<b>10.200</b>	<b>277.0</b>	<b>0.0210000</b>	<b>0.552</b>	<b>0.769000</b>	<b>3.60</b>	<b>7.38</b>	<b>5.51</b>	<b>2.76</b>

parameter model	$d_1$	$d_2$	$d_3$	$q_1$	$q_2$	$q_3$	$f_1$	$f_2$	$f_3$	ECS	TCR	$F_{2\times CO_2}$	$F_{4\times CO_2}$
<b>ACCESS-CM2</b>	0.635	7.76	319	0.131	0.495	0.794	-0.799	0	0.515	4.32	1.98	3.04	7.58
<b>ACCESS-ESM1-5</b>	2.34	66.6	1040000000	0.445	0.426	2.45e-06	4.83	0	0.00086	2.92	1.99	3.35	6.71
<b>AWI-CM-1-1-MR</b>	1.09	6.29	163	0.203	0.306	0.335	4.3	0	0.117	3.2	2.05	3.79	7.93
<b>BCC-CSM2-MR</b>	0.976	5.78	208	0.192	0.23	0.402	0.821	0	0.408	2.82	1.58	3.42	8.02
<b>BCC-ESM1</b>	2.21	15.2	353	0.373	0.328	0.519	2.07	0	0.171	3.21	1.76	2.63	5.76
<b>CAMS-CSM1-0</b>	0.577	4.92	135	0.0991	0.284	0.154	6.26	0	0.00235	2.34	1.73	4.36	8.72
<b>CESM2-FV2</b>	0.531	4.37	417	0.0862	0.448	1.26	2.0	0	0.278	5.97	2.01	3.32	7.45
<b>CESM2-WACCM</b>	0.328	4.88	326	0.0516	0.482	0.864	0.0334	0	0.468	4.6	1.93	3.29	7.94
<b>CESM2-WACCM-FV2</b>	0.621	6.51	458	0.132	0.485	1.16	3.17	0	0.132	5.54	2.04	3.12	6.62
<b>CMCC-CM2-SR5</b>	1.54	29.3	567000	0.337	0.368	0.00106	3.83	0	0.178	2.75	2.17	3.89	8.3
<b>CNRM-CM6-1</b>	1.8	24.7	754	0.324	0.442	5.81e-06	0.591	0	0.465	2.8	2.23	3.66	8.66
<b>CNRM-CM6-1-HR</b>	1.72	15.6	296	0.265	0.445	0.19	4.61	0	0.11	3.57	2.48	3.97	8.25
<b>CNRM-ESM2-1</b>	0.914	8.27	317	0.133	0.694	0.724	-1.04	0	0.429	3.53	1.86	2.28	5.79
<b>CanESM5</b>	1.22	11.1	289	0.227	0.602	0.779	2.06	0	0.257	5.18	2.63	3.22	7.19
<b>E3SM-1-0</b>	0.973	11.0	272	0.202	0.673	0.847	3.7	0	0.117	5.83	2.94	3.39	7.11
<b>FGOALS-g3</b>	0.88	5.03	240	0.15	0.307	0.34	0.403	0	0.422	2.57	1.54	3.23	7.67

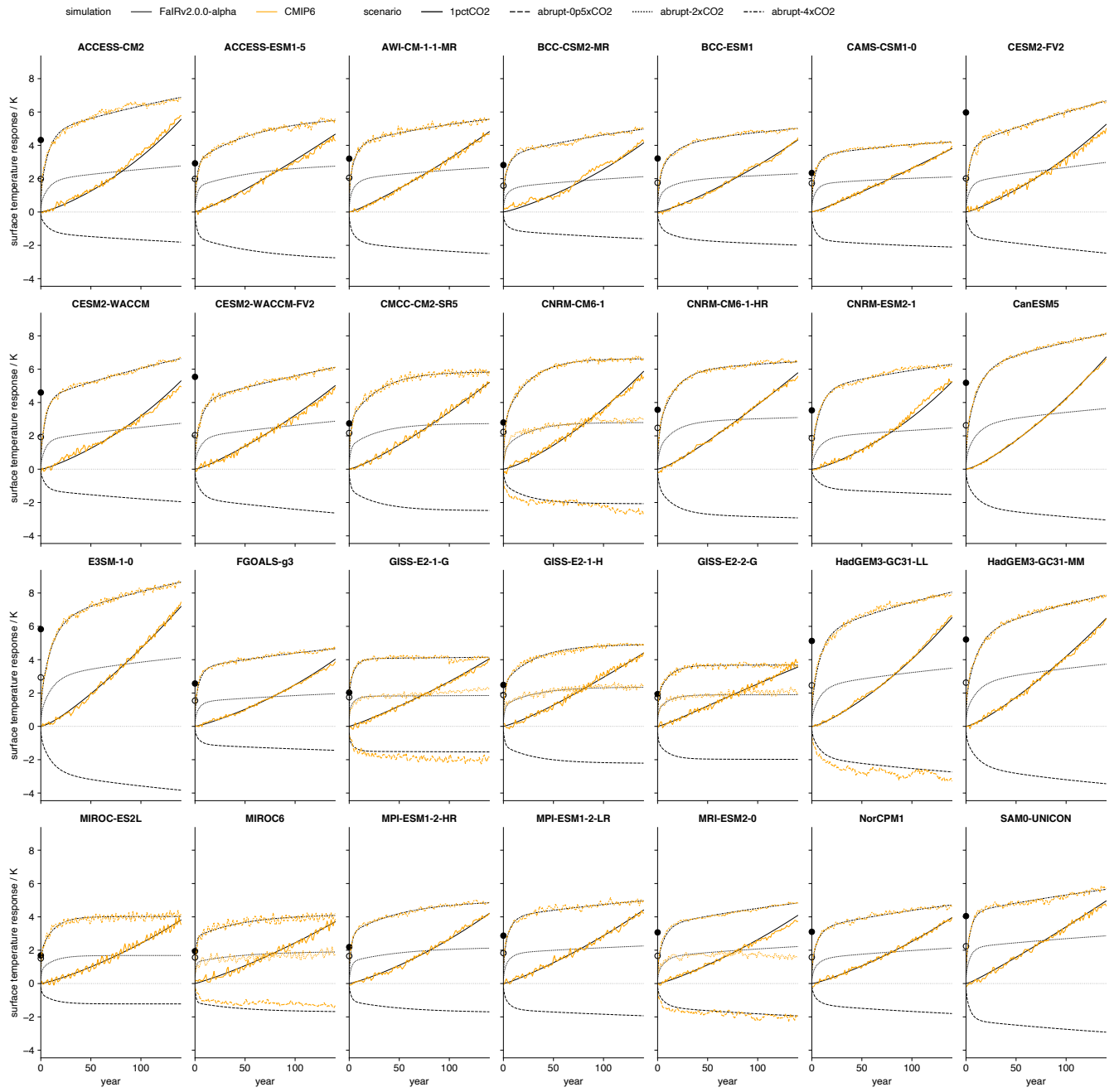


**Figure 3.** FaIRv2.0.0 emulation of CMIP6 model response to the abrupt-4xCO<sub>2</sub>, abrupt-4xCO<sub>2</sub>, abrupt-2xCO<sub>2</sub>, abrupt-0p5xCO<sub>2</sub>, and 1pctCO<sub>2</sub> experiments. Small black line shows FaIRv2.0-alpha emulation, orange and blue dots show drift-corrected line shows CMIP6 model surface temperature anomaly output for data where available. Emulation parameters were fit using the abrupt-4xCO<sub>2</sub> and 1pctCO<sub>2</sub> experiments respectively. Dashed black lines show corresponding FaIRv2.0 emulation so the abrupt-2xCO<sub>2</sub> and abrupt-0p5xCO<sub>2</sub> simulations can be considered as verification experiments for the models where the data for these experiments is available. Large orange filled and blue unfilled dots over the y-axis indicate the assessed model ECS and TCR respectively (see table Table 2).

We found that optimal parameters found over the first 150 years of the abrupt 4xCO<sub>2</sub> experiment were not able to well-reproduce the remainder of the experiment for those models that continued the experiment past 150 years (CESM2 and NorESM2-LM). These models appear to exhibit particularly high ocean heat uptake efficacy, resulting in a sharp “elbow” feature in their Gregory plots (see figure S2), which tends to be underestimated by the maximum likelihood procedure when tuning to abbreviated data. Without longer runs from more models, it is difficult to predict whether the projection issues with tuning parameters to the first 150 years observed in these two models would apply more generally. Rugenstein et al. (2020) suggests that the inclusion of an ocean heat uptake efficacy in the fit should alleviate this issue to a limited extent.

### 3.2 Tuning the carbon cycle response

We tune the carbon cycle using CMIP6 data from the C4MIP (Jones et al., 2016) fully coupled and biogeochemically coupled 1pctCO<sub>2</sub> runs (K. Arora et al., 2020). Since constraining the response coefficients  $a_i$  and timescales  $\tau_i$  requires pulse-emission experiments such as carried out by Joos et al. (2013), here we only fit the  $r$  feedback parameters and keep the response coefficients,  $a$ , and timescales,  $\tau$ , equal to the multi-model mean from Joos et al. (2013). The inclusion of both the fully coupled and biogeochemically coupled runs in the procedure allows us to constrain  $r_u$ ,  $r_a$ , and  $r_T$  independently. We use equations 2 and 3 to diagnose the values of  $\alpha$  required to reproduce the C4MIP emissions from the corresponding concentrations within the FaIRv2.0.0 carbon-cycle impulse-response framework. We then use equation 4 to convert  $\alpha$  into iIRF<sub>100</sub> timeseries. Finally, we use an ordinary least squares estimator to calculate  $r$  parameters by regressing the C4MIP cumulative uptake, temperature and atmospheric burden timeseries against the diagnosed iIRF<sub>100</sub> timeseries.  $r_0$  is taken as the intercept of the estimator. We include the atmospheric burden as a predictor (and hence obtain non-zero  $r_A$  values) due to a significant reduction in regression residual for several models when included. We find that all the C4MIP models display an exceptionally high, rapidly decreasing initial airborne fraction. In terms of the FaIRv2.0.0 equations, this corresponds to an  $\alpha$  value that decreases initially before reaching a minimum, representing a carbon sink that initially increases in strength when concentrations start to rise before decreasing as the concentrations and temperatures rise further. FaIRv2.0.0 is unable to fully capture this initial adjustment, and as such in our tunings we prioritise emulating the long-term behaviour and carry out the regression ~~over the final 75 years of the C4MIP data from year 60 onwards~~. It would be possible to better capture the initial adjustment by including additional terms in equation 4, but since it remains to be seen whether this behaviour is apparent in scenarios where concentrations do not rise suddenly and rapidly from a pre-industrial level as is the case in the 1pctCO<sub>2</sub> experiment (such as a historical emission scenario), we do not do so here. Tuned parameters are given ~~below, with figure in Table 3, with Figure 4 showing diagnosed C4MIP emissions and the FaIRv2.0.0-alpha emulation~~. We note that these tunings suggest that the pre-industrial sink strength (which is encapsulated by  $r_0$ ) in ~~all but one of the 7/11~~ models is higher than the historically observed best-estimate found here (2.1.1), and in a previous study (Jenkins et al., 2018). ~~r<sub>0</sub> r<sub>u</sub> r<sub>T</sub> r<sub>a</sub> ACCESS-ESM1-5 32.8 -0.048200 3.4400 -0.00627 BCC-CSM2-MR 27.7 0.001590 4.5200 0.00873 CESM2 41.3 0.007510 1.1900 0.00626 CNRM-ESM2-1 38.5 -0.000362 2.4400 0.01030 CanESM5 35.9 -0.007120 -0.0847 0.01910 GFDL-ESM4 35.8 0.017700 4.5100 -0.00156 IPSL-CM6A-LR 34.8 0.009360 0.9340 0.01560 MIROC-ES2L 34.3 0.010400 3.2900 0.00574 MPI-ESM1-2-LR 35.7 0.020800 1.2600 0.00357 NorESM2-LM 41.3 0.005590 1.4500 0.00757 UKESM1-0-LL 38.5 0.018100 2.5800 0.00287~~

**Table 3.** Tuned CMIP6 carbon-cycle parameters.

<b>parameter</b> <b>model</b>	$r_0$	$r_u$	$r_T$	$r_a$
<b>ACCESS-ESM1-5</b>	36.7	0.035	3.04	-0.00066
<b>BCC-CSM2-MR</b>	25.6	0.00598	5.2	0.00439
<b>CESM2</b>	40.7	0.0107	1.28	0.00421
<b>CNRM-ESM2-1</b>	38.1	0.000581	2.47	0.00978
<b>CanESM5</b>	35.7	-0.00596	-0.104	0.0181
<b>GFDL-ESM4</b>	34.3	0.0219	4.86	-0.00424
<b>IPSL-CM6A-LR</b>	32.2	0.0166	1.07	0.0123
<b>MIROC-ES2L</b>	33.4	0.0131	3.46	0.00399
<b>MPI-ESM1-2-LR</b>	33.3	0.031	1.5	-0.00257
<b>NorESM2-LM</b>	40.7	0.00947	1.56	0.00489
<b>UKESM1-0-LL</b>	37.9	0.0201	2.67	0.00181

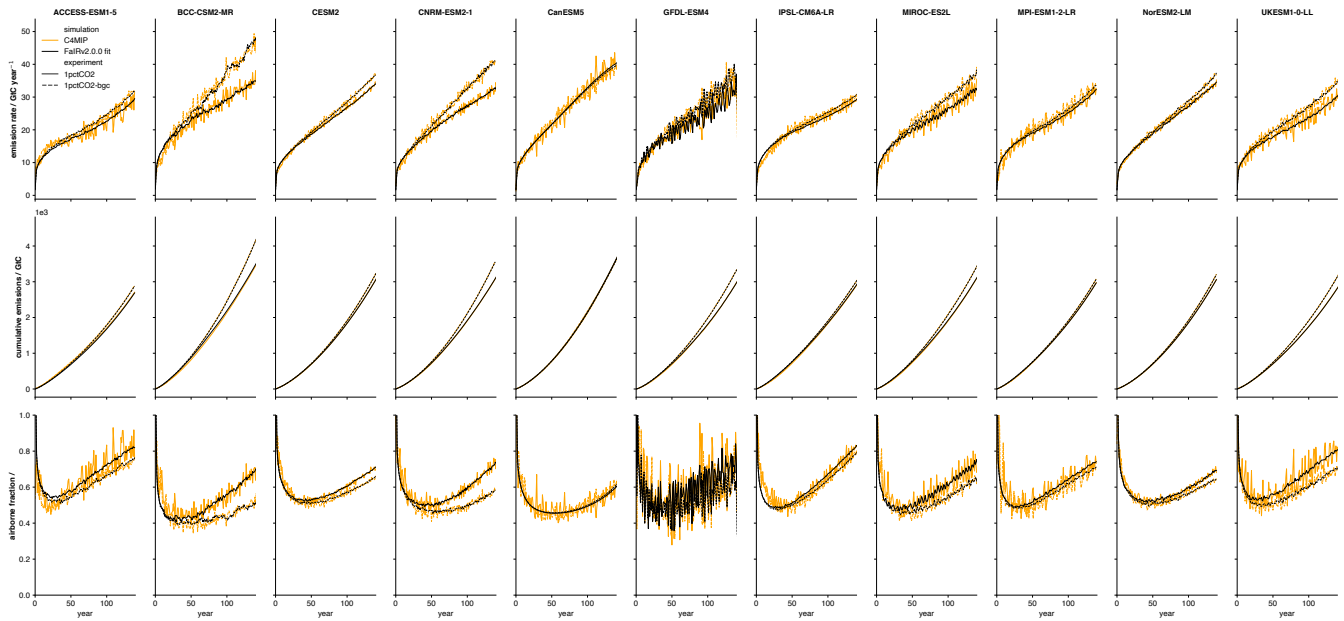


**Figure 4.** FaIRv2.0.0 emulation of CMIP6 model carbon cycle response to the C4MIP 1pctCO<sub>2</sub> experiments. Orange and blue dots show model annual and cumulative emissions for the experiments specified above the figure. Dashed black lines show corresponding Black line shows FaIRv2.0.0-alpha emulation, and orange line shows C4MIP model data. Red dots in the right-hand column show Top row shows diagnosed emission rates, middle row cumulative emissions arising from radiation feedback directly from, and bottom row airborne fraction. Solid line indicates the radiatively-coupled 1pctCO<sub>2</sub> experiment fully coupled C4MIP runs, while blue dots dashed lines show cumulative emissions calculated as the difference between the equivalent fully- and biogeochemically-coupled experiments biogeochemically coupled runs (emulated in FaIRv2.0.0-alpha by setting  $r_T = 0$ ).

### 3.3 Tuning aerosol ERF

Aerosol forcing relationships are tuned to ERF data from 10 CMIP6 models and emission data from the RCMIP protocol (Nicholls et al., 2020a) following Smith et al. (2020). For each CMIP6 model, aerosol-radiation and aerosol-cloud interaction components of the ERF are calculated by the Approximate Partial Radiative Perturbation (APRP) method. For additional details on the exact procedure, see Smith et al. (2020) and Zelinka et al. (2014). For each model, we fit the  $f$  coefficients in equation 6 to the ERF<sub>ari</sub> component using an ordinary least squares estimator. The resulting coefficients are almost identical to those from Smith et al. (2020), with differences arising only due to the emission data used. We then fit the  $f$  coefficients and  $C_0^{SO_2}$  in equation 7 to the ERF<sub>aci</sub> component by minimising the residual sum of squares using a simplex algorithm (Nelder and Mead, 1965). The tuned parameters are given ~~below~~ in Table 4. Figure 5, following ~~figure~~ Figure 2 of Smith et al. (2020), shows the parameterised fits compared to the APRP derived model ERF components.

$f_2^{BC}$   $f_2^{OC}$   $f_2^{SO_2}$   $f_1^{aci}$   
 $C_0^{SO_2}$   $f_2^{aci}$  CanESM5 0.03260 -0.000347 -0.002490 -0.387 23.8 -0.015200 E3SM 0.02480 -0.012600 -0.000942 -1.640 113.0  
-0.014200 GFDL-CM4 0.02690 -0.002090 -0.002610 -2.230 427.0 -0.008030 GFDL-ESM4 0.10200 -0.030400 -0.002640  
-57.600 17000.0 -0.015300 GISS-E2-1-G 0.14600 -0.044100 -0.006680 -0.156 16.8 -0.017600 HadGEM3-GC31-LL 0.00196  
0.004150 -0.002910 -0.783 66.9 -0.006910 IPSL-CM6A-LR -0.05610 0.008850 -0.000748 -0.951 306.0 -0.001730 MIROC6  
0.03870 -0.014200 -0.001780 -0.392 46.6 -0.012400 NorESM2-LM 0.00302 -0.003400 -0.001260 -68.600 10300.0 -0.012300  
UKESM1-0-LL 0.00255 0.000063 -0.002390 -0.740 38.9 -0.000265

**Table 4.** Tuned CMIP6 aerosol forcing parameters.

source	ERFari			ERFaci		
parameter	$f_2^{\text{SO}_2}$	$f_2^{\text{BC}}$	$f_2^{\text{OC}}$	$f_1^{\text{aci}}$	$C_0^{\text{SO}_2}$	$f_2^{\text{aci}}$
model						
<b>CanESM5</b>	-0.00249	0.0326	-0.000347	-0.387	23.8	-0.0152
<b>E3SM</b>	-0.000942	0.0248	-0.0126	-1.64	113	-0.0142
<b>GFDL-CM4</b>	-0.00261	0.0269	-0.00209	-2.23	427	-0.00803
<b>GFDL-ESM4</b>	-0.00264	0.102	-0.0304	-57.6	17000	-0.0153
<b>GISS-E2-1-G</b>	-0.00668	0.146	-0.0441	-0.156	16.8	-0.0176
<b>HadGEM3-GC31-LL</b>	-0.00291	0.00196	0.00415	-0.783	66.9	-0.00691
<b>IPSL-CM6A-LR</b>	-0.000748	-0.0561	0.00885	-0.951	306	-0.00173
<b>MIROC6</b>	-0.00178	0.0387	-0.0142	-0.392	46.6	-0.0124
<b>NorESM2-LM</b>	-0.00126	0.00302	-0.0034	-68.6	10300	-0.0123
<b>UKESM1-0-LL</b>	-0.00239	0.00255	6.32e-05	-0.74	38.9	-0.000265

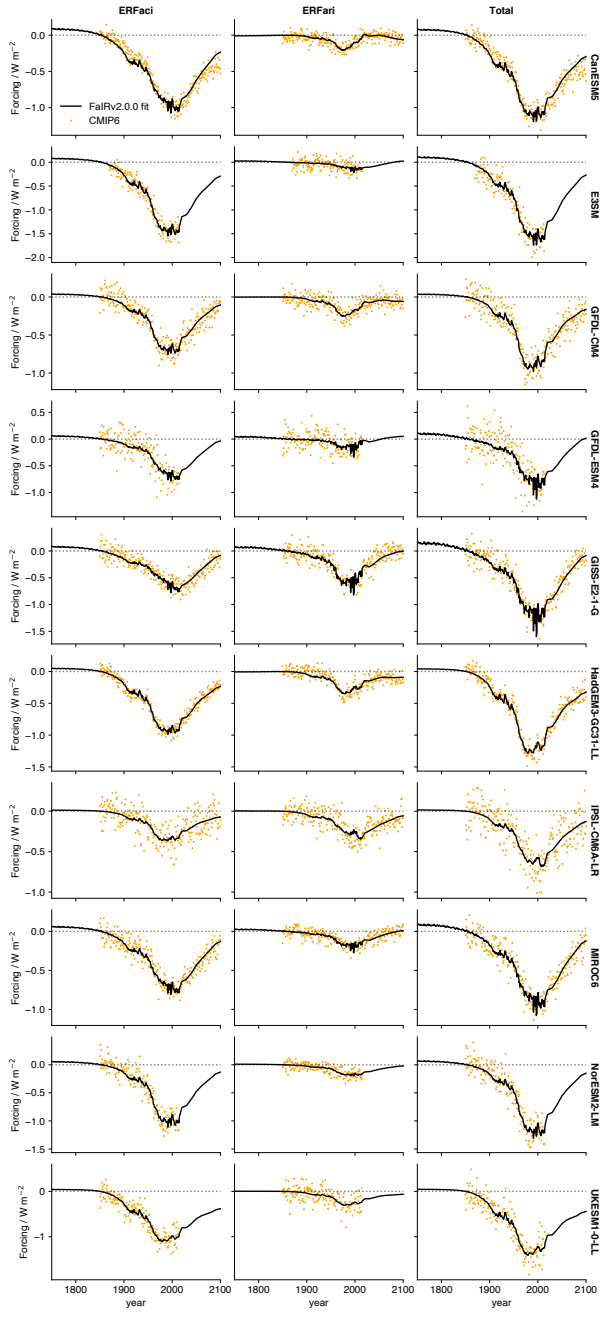


**Figure 5.** Top row shows entire CMIP6 model ensemble compared to the FULL and CONSTRAINED FaIRv2.0 parameter ensembles described in 4. All other figures show FaIRv2.0 emulation of individual CMIP6 models. Orange dots show CMIP6 model output derived using APRa aerosol forcing. Black dashed line shows FaIRv2.0.0-alpha emulation, and orange dots show CMIP6 model data. All series displayed are relative to zero effective radiative forcing in 1850.

## 4 Constraining probabilistic parameter ensembles

The computational efficiency of SCMs makes them an ideal tool for carrying out large ensemble simulations from which probabilistic projections can be derived. Smith et al. (2018) carried out such a large ensemble, and produced projections  
485 based on constraining the ensemble members to fall within the 5-95% uncertainty range in observed warming to date from the Cowtan and Way dataset (Cowtan and Way, 2014). Here we replicate this procedure with the new model, but ~~with an additional constraint on the current rate of warming using a new constraint methodology~~, and updated prior parameters distributions.

### 4.1 The current level and rate of warming

We determine the current level and rate of warming following the Global Warming Index methodology (Haustein et al., 2017).  
490 This takes into account multiple sources of uncertainty: observational, forcing, earth system response (through parameter variation in an identical ~~thermal~~-climate response model to the one used in ~~FaIR~~FaIRv2.0.0) and internal variability. ~~We find that a 90%~~ credible interval on the 2014 level of warming relative to 1861–1880 is 0.75–1.26 K; and on the 2010–2014 rate of warming is 0.18–0.40 K decade<sup>-1</sup>. We use 2014 as the year in which our constraint is applied as this is With this methodology, we obtain an estimate of the distribution of the final year for which historical aerosol emissions—used in the calculation of the  
495 forcing timeseries—are available (Hoesly et al., 2018). We could extend the calculation to the present day using the SSP2-4.5 emission scenario as was done in Smith et al. (2020), but the rapid reduction in sulfate emissions following 2014 in this scenario current (2010–19) level and rate of the anthropogenic contribution to global warming (the anthropogenic warming index distribution). A key choice within this estimate is the observational data product used. There are six widely-used products available  
500 (Lenssen et al., 2019; Cowtan and Way, 2014; Vose et al., 2012; Morice et al., 2011; Rohde et al., 2013; Morice et al., 2020). Here we average over the distributions implied by each product to obtain our final distribution used to constrain our FaIRv2.0.0 ensemble. This choice clearly projects significantly onto ~~the rate of warming constraint and this decline does not appear to reflect observed aerosol forcing trends from atmospheric reanalyses (Bellouin et al., 2020a)~~. We note that the interval obtained for the level of warming here is larger than previous estimates (Haustein et al., 2017; Leach et al., 2018); this is largely due to updates  
505 to the aerosol forcing timeseries our results, so we provide results for each dataset in turn in Section 4.3.5 to demonstrate the sensitivity of our analysis to the choice of dataset. For full details of ~~the~~ this calculation, see the supplement.

#### 4.1.1 Definition of global mean temperature

Recent studies (Richardson et al., 2016, 2018) have shown that the definition of globally averaged surface temperature used is important when comparing observations to climate model output, and is relevant when exploring policy-relevant quantities such as the carbon budget (Tokarska et al., 2019). Discrepancies arise since observations blend air temperatures over  
510 land and sea ice with water temperature over ocean, and do not have full global coverage (they are blended-masked); while climate model surface temperature output is globally complete, and always measured as the air temperature 2m above the surface of the Earth. It has been shown both historically, and over future climate scenarios (Richardson et al., 2018), that the blended-masked temperature definition (GMST) may be cooler than the globally complete 2m air temperature definition

(GSAT). In our Global Warming Index calculation, we use the mean of 5 (4.1), we combine 6 temperature observation datasets (Lenssen et al., 2019; Cowtan and Way, 2014; Vose et al., 2012; Morice et al., 2011; Rohde et al., 2013) following the IPCC Special Report on 1.5°C warming (IPCC, 2018) (Lenssen et al., 2019; Cowtan and Way, 2014; Vose et al., 2012; Morice et al., 2011; Rohde et al., 2013); this implies that our constrained ensemble will broadly measure surface temperatures using the GMST definition. This will may lead to slightly lower model estimates of surface temperature than if we used the GSAT definition. We can estimate the difference between our definition of GMST and GSAT by regressing the 5-dataset 6-dataset mean used here against GSAT from ERA5 (Hersbach et al., 2020). A least squares estimator [confidence calculated using a block-bootstrap (Wilks, 1997)] suggests that our GMST definition is  $3.4 \pm 0.01$  4.6 [0.4, 10.8] % smaller than GSAT<sup>2</sup>.

## 4.2 Sampled prior distributions

### 4.2.1 Carbon cycle parameters

While including the atmospheric burden is necessary to well-emulate the carbon-cycle behaviour of individual C4MIP models, parameterising the iIRF<sub>100</sub> as a linear function of just cumulative carbon uptake and temperature is sufficient to capture the spread of the model ensemble. Correlations between parameters also complicate sampling from the inferred parameter distributions derived from table Table 3. We therefore repeat the parameter tuning procedure described in section Section 3.2, but exclude the atmospheric burden as a predictor for the C4MIP iIRF<sub>100</sub> timeseries. The resulting  $r_0$ ,  $r_u$  and  $r_T$  parameter samples are uncorrelated. We sample these parameters by applying scaling factors inferred from the CMIP6 tunings to the default parameter values (for  $r_u$  and  $r_T$  this is equivalent to sampling directly from the distribution inferred from the CMIP6 tunings). The underlying uncorrelated scaling factor distributions are given below: parameter default value scaling factor,  $X$ :  $r_0 = 30.4$ ,  $X \sim \mathcal{N}(1, 0.122)$ ;  $r_u = 0.0177$ ,  $\ln(X) \sim \mathcal{N}(0, 0.116)$ ;  $r_T = 2.64$ ,  $X \sim \mathcal{N}(1, 0.613)$  in Table 5.

**Table 5.** Carbon-cycle parameter sampling.

parameter	default value	scaling factor, $X$
$r_0$	33.9	$X \sim \mathcal{N}(1, 0.154)$
$r_u$	0.0188	$\ln(X) \sim \mathcal{N}(0, 0.442)$
$r_T$	2.67	$X \sim \mathcal{N}(1, 0.615)$

<sup>2</sup>square brackets indicate a 90% credible interval

#### 4.2.2 Forcing parameters

Uncertainty in effective radiative forcing is included by grouping individual forcing agents into broader forcing classes (IPCC  
535 et al., 2013), and applying a randomly sampled scaling factor to all the  $f$  parameters within each class (with the exception  
of aerosol forcings, which we discuss [immediately below](#)). Scaling factors between forcing classes are uncorrelated. The  
scaling factor distributions ~~are given below~~[used for each forcing class are given in Table 6](#). Uncertainty in aerosol forcing is  
included as follows. ERFari  $f$  coefficients (equation 6) are first drawn from a multivariate normal distribution inferred from  
the CMIP6 tuned parameters in [Table 4](#). We then apply a quantile map to scale the resulting coefficients such that the 1850  
540 to 2005-2015 mean ERFari distribution matches the process based assessment in Bellouin et al. (2020b). For ERFaci,  $f_2^{aci}$   
coefficients (equation 7) are drawn from a normal distribution inferred from the CMIP6 tuned parameters in [Table 4](#).  $f_1^{aci}$   
and  $C_0^{SO_2}$  coefficients are drawn from a multivariate log-normal distribution; this ensures we sample the full range of ERFaci  
shapes provided by CMIP6 models. As with the ERFari coefficients, we then apply a quantile map to scale these coefficients  
such that the sampled 1850 to 2005-2015 mean ERFaci distribution matches Bellouin et al. (2020b). ~~The underlying scaling  
545 factor distributions used for each forcing class (excluding aerosol forcing) are given below.~~[forcing category scaling factor,  \$X\$](#)   
~~5-95% uncertainty (%)~~  
~~CO<sub>2</sub>  $X \sim \mathcal{N}(1, 0.122) \pm 20$~~   
~~CH<sub>4</sub>  $X \sim \mathcal{N}(1, 0.170) \pm 28$~~   
~~N<sub>2</sub>O  $X \sim \mathcal{N}(1, 0.122) \pm 20$~~ [other WMGHGs](#)  
~~X  $\sim \mathcal{N}(1, 0.122) \pm 20$~~   
~~tropospheric ozone  $X \sim \mathcal{N}(1, 0.304) \pm 50$~~   
~~stratospheric ozone  $X \sim \mathcal{N}(1, 1.22) \pm 200$~~   
~~stratospheric H<sub>2</sub>O from CH<sub>4</sub>  $X \sim \mathcal{N}(1, 0.438) \pm 72$~~   
~~black carbon on snow ln(X)  $\sim \mathcal{N}(0, 0.457)$~~   
~~contrails  $X \sim \mathcal{N}(1, 0.456) \pm 75$~~   
~~land use change  $X \sim \mathcal{N}(1, 0.456) \pm 75$~~   
~~volcanic  $X \sim \mathcal{N}(1, 0.304) \pm 50$~~   
~~solar  $X \sim \mathcal{N}(1, 0.608) \pm 100$~~

**Table 6.** ERF parameter sampling.

forcing category	scaling factor, $X$	5-95% uncertainty (%)
CO <sub>2</sub>	$X \sim \mathcal{N}(1, 0.122)$	±20
CH <sub>4</sub>	$X \sim \mathcal{N}(1, 0.170)$	±28
N <sub>2</sub> O	$X \sim \mathcal{N}(1, 0.122)$	±20
other WMGHGs	$X \sim \mathcal{N}(1, 0.122)$	±20
ozone	$X \sim \mathcal{N}(1, 0.304)$	±50
stratospheric H <sub>2</sub> O from CH <sub>4</sub>	$X \sim \mathcal{N}(1, 0.438)$	±72
black carbon on snow	$\ln(X) \sim \mathcal{N}(0, 0.457)$	-
contrails	$X \sim \mathcal{N}(1, 0.456)$	±75
land use change	$X \sim \mathcal{N}(1, 0.456)$	±75
volcanic	$X \sim \mathcal{N}(1, 0.304)$	±50
solar	$X \sim \mathcal{N}(1, 0.608)$	±100

## 550 4.2.3 Thermal response parameters

Uncertainty in thermal response is incorporated by sampling response parameters directly from distributions inferred from the CMIP6 tunings in section-Section 2, taking correlations between parameters into account. Referring to parameters as in equations 10, 11, 12 and 13, we draw parameters from the following distributions.  $d_1$ ,  $d_2$  and  $q_1$  are highly correlated, and we therefore sample  $\ln(d_1)$ ,  $\ln(d_2)$  and  $q_1$  from a multivariate normal distribution with covariances and means taken from the values in section-Section 2.  $d_3$  is not strongly correlated with any other parameter, and so we sample  $\ln(d_3)$  from a normal distribution. We then independently sample the TCR and the TCR/ECS ratio, the Realised Warming Fraction (RWF); as it has been shown that the TCR and RWF are much more weakly correlated than any other combination of ECS, TCR and RWF (Millar et al., 2015). We draw TCR samples from a normal distribution,  $\text{TCR} \sim \mathcal{N}(2, 0.608)$ , truncating the distribution at a distance of  $\pm 3\sigma$  from the central value of 2. We draw RWF samples from a normal distribution  $\text{RWF} \sim \mathcal{N}(0.55, 0.15)$ , again truncating at  $\pm 3\sigma$ . The 90% credible interval of the sampled TCR and RWF distributions closely, but not exactly, match the ranges inferred from the parameters in table-Table 2. Using equations 12 and 13, we then calculate  $q_2$  and  $q_3$ . We reject any samples in which any of the  $q$  parameters are unphysical (negative). The quantiles of the underlying prior ECS and TCR distributions used are given below in Table 7.

## 4.3 The constrained ensemble

565 Taking historical CO<sub>2</sub> emissions from GCP (Friedlingstein et al., 2019), and all other historical and future SSP (Riahi et al., 2017) emissions from the RCMIP protocol (Nicholls et al., 2020a); and land use change, volcanic, and solar forcing from the SSP effective radiative forcing timeseries (Smith, 2020), we run a 1,000,000 member emission-driven ensemble (FULL), sampling uncertainty in the carbon cycle, effective radiative forcing and thermal response as described above. We then constrain this ensemble (CONSTRAINED) based on the assessed 90% credible intervals of the 2014 in Sections 4.2.1, 4.2.2, and 4.2.3. 570 This FULL ensemble is then constrained by setting the selection probability of each member equal to the likelihood of its simulated present-day level and rate of the Global Warming Index (Haustein et al., 2017) as above (4.1) anthropogenic warming within the anthropogenic warming index distribution. These likelihoods are calculated using a binning procedure at a resolution of 0.01 K (level) and 0.001 K year<sup>-1</sup> (rate). Finally, we subsample the FULL ensemble based on these selection probabilities to generate the CONSTRAINED ensemble. This procedure retains 9.6 % of the FULL ensemble. Table 7 gives outlines the 575 results of this analysis in terms of the quantiles of key variables metrics: the model climate sensitivity and present-day radiative forcing.

**Table 7.** Constrained ensemble results for climate sensitivities and current ERF. ERF in 2019 is based on following an SSP2-4.5 pathway from 2014 onwards.

	ensemble percentile	FULL					CONSTRAINED				
		5%	16.6%	50%	83.3%	95%	5%	16.6%	50%	83.3%	95%
<b>climate sensitivities / K</b>	<b>ECS</b>	1.80	2.45	3.69	5.66	8.05	1.94	2.36	3.24	4.74	6.59
	<b>TCR</b>	1.14	1.48	2.03	2.60	3.01	1.30	1.48	1.79	2.15	2.44
<b>2019 ERF components / W m<sup>-2</sup></b>	<b>CO<sub>2</sub></b>	1.61	1.81	2.12	2.45	2.69	1.67	1.86	2.15	2.46	2.70
	<b>CH<sub>4</sub></b>	0.45	0.52	0.62	0.73	0.80	0.45	0.52	0.62	0.72	0.79
	<b>N<sub>2</sub>O</b>	0.16	0.17	0.20	0.22	0.24	0.16	0.17	0.20	0.22	0.24
	<b>other WMGHGs</b>	0.29	0.32	0.36	0.40	0.43	0.29	0.32	0.36	0.40	0.43
	<b>ozone</b>	0.24	0.33	0.47	0.61	0.70	0.23	0.33	0.47	0.60	0.70
	<b>stratospheric H<sub>2</sub>O from CH<sub>4</sub></b>	0.01	0.03	0.05	0.07	0.09	0.01	0.03	0.05	0.07	0.09
	<b>aerosol-radiation interaction</b>	-0.60	-0.47	-0.30	-0.15	-0.03	-0.59	-0.47	-0.31	-0.16	-0.06
	<b>aerosol-cloud interaction</b>	-2.28	-1.48	-0.70	-0.26	-0.05	-1.16	-0.90	-0.55	-0.27	-0.10
	<b>total aerosol</b>	-2.63	-1.81	-1.02	-0.53	-0.27	-1.47	-1.22	-0.88	-0.57	-0.36
	<b>black carbon on snow</b>	0.04	0.06	0.09	0.14	0.19	0.04	0.06	0.09	0.13	0.18
<b>total anthropogenic</b>	<b>contrails</b>	0.01	0.03	0.06	0.08	0.10	0.01	0.03	0.06	0.08	0.10
	<b>albedo from land use change</b>	-0.35	-0.29	-0.20	-0.11	-0.05	-0.35	-0.29	-0.20	-0.11	-0.05
	<b>total anthropogenic</b>	1.01	1.86	2.73	3.39	3.81	2.19	2.47	2.90	3.35	3.68
climate sensitivity 5% 17% 50% 83% 95% 5% 17% 50% 83% 95% ECS 1.91 2.55 3.73 5.43 7.26 1.94 2.36 3.17 4.45 5.84 TCR 1.18 1.53											
<b>2.06 2.62 3.02 1.25 1.45 1.77 2.13 2.41 2019 ERF relative to 1750 / W m<sup>-2</sup></b>	<b>CO<sub>2</sub> 1.62 1.80 2.08 2.37 2.58 1.67 1.84 2.11 2.38 2.59 CH<sub>4</sub> 0.45 0.53 0.63 0.73 0.81 0.45 0.52 0.63 0.73 0.80 N<sub>2</sub>O 0.16 0.18 0.20 0.22 0.24 0.16 0.18 0.20 0.22 0.24 other WMGHGs 0.29 0.32 0.36 0.40 0.43 0.29 0.32 0.36 0.40 0.43 tropospheric O<sub>3</sub> 0.20 0.28 0.40 0.51 0.59 0.20 0.28 0.39 0.51 0.59 stratospheric O<sub>3</sub> 0.14 0.10 0.05 0.01 0.05 0.14 0.10 0.05 0.01 0.05 stratospheric H<sub>2</sub>O from CH<sub>4</sub> 0.02 0.04 0.06 0.09 0.11 0.02 0.04 0.06 0.09 0.11 total WMGHGs 3.14 3.36 3.69 4.02 4.27 3.18 3.39 3.71 4.03 4.27 ERFari -0.59 -0.46 -0.30 -0.14 -0.02 -0.58 -0.46 -0.31 -0.16 -0.05 ERFaci -2.26 -1.46 -0.69 -0.26 -0.05 -1.25 -1.00 -0.63 -0.30 -0.11 total aerosols -2.59 -1.79 -1.00 -0.52 -0.26 -1.56 -1.32 -0.95 -0.60 -0.37 black carbon on snow 0.04 0.05 0.09 0.13 0.18 0.04 0.05 0.08 0.13 0.18 contrails 0.01 0.02 0.04 0.06 0.07 0.01 0.02 0.04 0.06 0.07 total anthropogenic 0.90 1.73 2.59 3.22 3.63 1.98 2.25 2.67 3.13 3.46</b>										

### 4.3.1 Current effective radiative forcing

The constraint applied only significantly affects the estimated ranges of ERFaci, total aerosol and anthropogenic forcings in 2019 (based on an SSP2-45 pathway following 2014). ERFaci is constrained from -0.69 -0.70 [-2.26 -2.28 , -0.05] <sup>3</sup> to -0.63

580 to -0.55 [-1.25 , -0.11 -1.16 , -0.10]; total aerosol forcing from -1.00 -1.02 [-2.59 , -0.26 -2.63 , -0.27] to -0.95 -0.88 [-1.55  
-0.37 -1.47 , -0.36]; and total anthropogenic forcing from 2.59 -2.73 [0.90 , 3.63 1.01 , 3.81] to 2.67 -2.90 [1.98 , 3.46 2.19 ,  
3.68]. These results are consistent with a recent study that used similar methods but concentrated on aerosol forcing and used a constraint based on observed warming and Earth energy uptake (Smith et al., 2020). Other forcing categories are not affected by the constraint due to their relatively smaller magnitude and/or prior uncertainty.

### 585 4.3.2 Climate sensitivities

We find that the TCR is constrained from 2.06 -2.03 [1.18 , 3.02 1.14 , 3.01] to 1.77 -1.79 [1.25 , 2.41 1.30 , 2.44] and the ECS from 3.73 -3.69 [1.91 , 7.26 1.80 , 8.05] to 3.17 -3.24 [1.94 , 5.84 6.59]. These results are relatively consistent with several recent studies that have used emergent constraint techniques (Nijssse et al., 2020; Jiménez-de-la Cuesta and Mauritsen, 2019; Tokarska et al., 2020) (Nijssse et al., 2020; Jiménez-de-la Cuesta and Mauritsen, 2019; Tokarska et al., 2020; Brunner et al., 2020; Ribes et al., 2021, Figure 6) 590 or drawn on multiple lines of evidence (Sherwood et al., 2020); our constrained likely range of TCR exactly matches Sherwood et al. to two significant places. The largest discrepancies with these studies occur at the upper tails of the constrained distributions ECS distribution; the constraint applied here is unable to rule out some higher values of the ECS which some of these other studies have done, though we note that the 95<sup>th</sup> percentile of the CONSTRAINED ECS distribution is only slightly above the robust upper bound in Sherwood et al. (2020). The CONSTRAINED RWF distribution does not differ significantly from the FULL 595 distribution of 0.55 [0.3 , 0.8].

---

<sup>3</sup> square brackets indicate a 90% credible interval

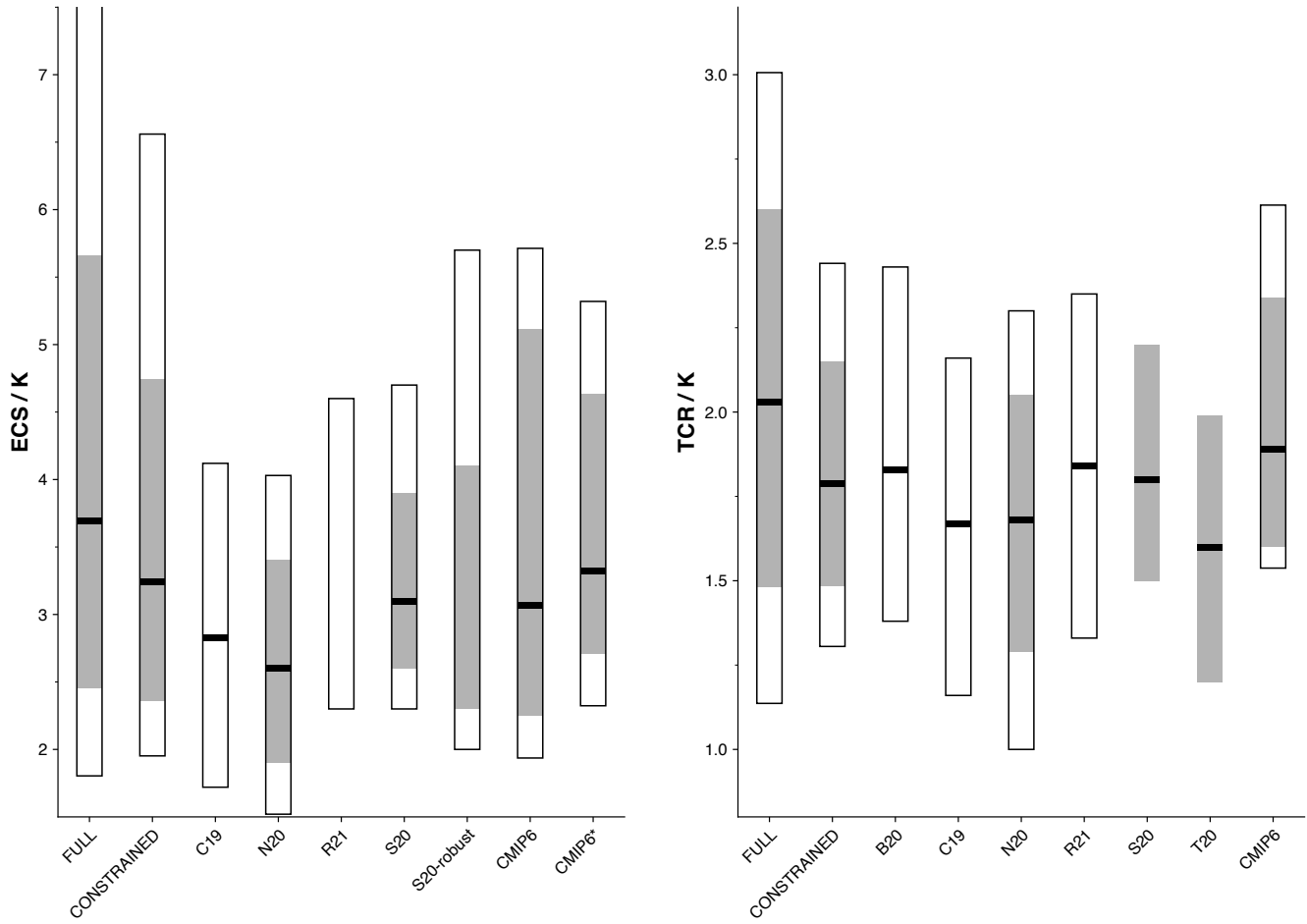


**Figure 6.** Climate sensitivities of our FULL, CONSTRAINED and ALTERNATIVE CONSTRAINED ensembles in the context of other studies. Black line indicates median values; grey shading likely range; unfilled bars 5-95% range. Studies included are: Nijssse et al. (2020); Tokarska et al. (2020); Jiménez-de-la Cuesta and Mauritsen (2019); Sherwood et al. (2020) Brunner et al. (2020, B20), Jiménez-de-la Cuesta and Mauritsen (2019, C19), Nijssse et al. (2020, N20), Ribes et al. (2021, R21), Sherwood et al. (2020, S20), Tokarska et al. (2020, T20). CMIP6 indicates climate sensitivities derived from the energy balance model fits calculated above in Section 3.1 (including ocean heat uptake efficacy), CMIP6\* indicates climate sensitivities derived using the Gregory method (Gregory et al., 2004) over the first 150 years of the abrupt-4xCO<sub>2</sub> experiment.

#### **4.3.3 Correlations between climate sensitivities and ERF**

There are significant correlations between key variables in the CONSTRAINED ensemble, consistent with previous studies (Smith et al., 2018; Millar et al., 2015; Sanderson, 2020; Forest et al., 2002; Marvel et al., 2016). These are shown in the contour plots in [figure](#)-Figure 7.

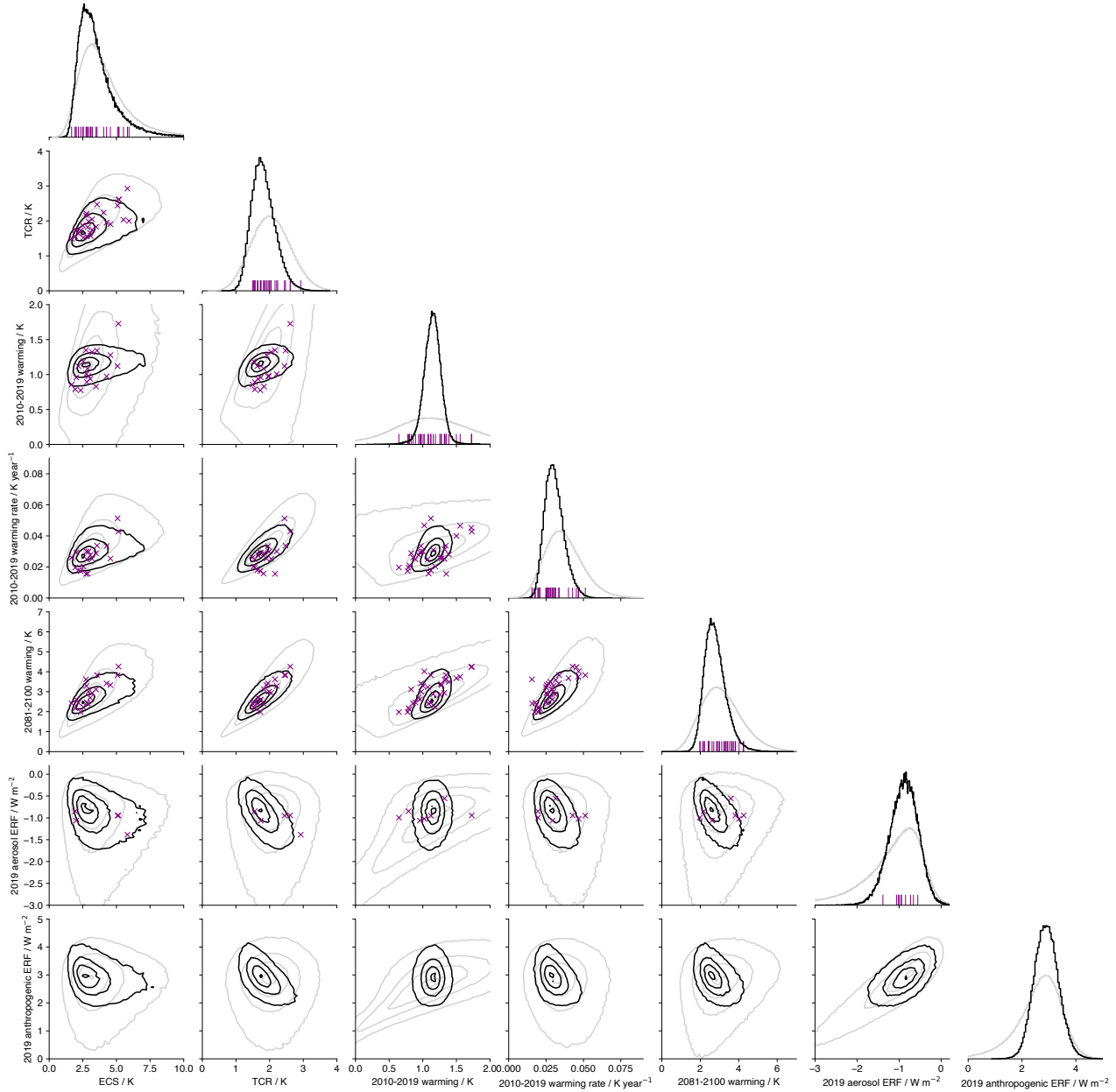


**Figure 7.** Corner plot depiction of key quantities within the FULL and CONSTRAINED ensembles, based on following a historical trajectory to 2014 and SSP2-45 thereafter. Diagonal plots show marginal probability density functions of each key variable; FULL shown in grey, CONSTRAINED in black, and FULL constrained by the current level of warming only in red. Subdiagonal plots show contour plots of gaussian kernel density estimates of joint probability density function. Contours shown indicate regions containing 95, 67 normalised likelihoods of 5, 33, 66 and 95 % of the ensemble members. Purple crosses and lines indicate the positions of individual CMIP6 models. The temperature and ERF variables are based 2010-2019 warming rate for CMIP6 models is calculated as the slope of a linear regression over 2000-2029 due to internal variability projecting strongly on following an SSP2-45 trajectory from 2014 onwards the slope estimate and error if a shorter period is used.

600 **4.3.4 Sensitivity to prior response parameter distributions**

Previous work has shown that posterior marginal distributions of ECS and TCR depend strongly on the assumed prior distributions (Bodman and Jones, 2016). Here we test the sensitivity of our CONSTRAINED results to the response parameters sampled in FULL by replacing the TCR and RWF sample distributions stated in [Section 4.2.3](#) with:  $\text{TCR} \sim \mathcal{U}(0.5, 3.5)$  and  $\text{RWF} \sim \mathcal{U}(0.2, 0.85)$ . The actual prior distributions of TCR and RWF differ slightly from those stated here due to the rejection of unphysical response parameter sets, which tends to occur more often for lower values of TCR and higher values of RWF: the quantiles of the ALT input TCR and ECS distributions are  $2.24$ ,  $2.17$  [ $0.87$ ,  $0.85$ ,  $3.37$ ] and  $4.11$ ,  $4.03$  [ $1.44$ ,  $10.55$ ,  $1.38$ ,  $10.46$ ] respectively. The posterior distributions of TCR and ECS after applying the constraint ([ALTERNATIVE ALT-CONSTRAINED](#)) described in [4.1](#) are [1.69](#) [Section 4.1](#) are  $1.73$  [ $1.15$ ,  $2.54$ ,  $1.21$ ,  $2.59$ ] and  $3.14$ ,  $3.28$  [ $1.74$ ,  $7.42$ ,  $1.82$ ,  $7.63$ ]. The resulting marginal posterior distributions are wider than in the CONSTRAINED ensemble; though not considerably so for the TCR estimate. The upper end of the [ALTERNATIVE ALT-CONSTRAINED](#) ECS distribution is most affected by the change in prior, suggesting that the current level and rate of warming does not provide an exceptionally tight constraint on the upper bound of the ECS. The [ALTERNATIVE ALT-CONSTRAINED](#) TCR distribution is not significantly different from CONSTRAINED, differing only by 0.1 K over the range of the distribution, demonstrating the close relationship between the TCR and historical warming (Sanderson, 2020) that enforces a tight constraint even with a significantly less informed prior. [An analogous figure to figure 7 but for the ALTERNATIVE ensemble is in the Supplement \(figure S3\).](#)

**Table 8.** Results for the key metrics under a less informed climate sensitivity prior.

	ensemble percentile	ALT					ALT-CONSTRAINED				
		5%	16.6%	50%	83.3%	95%	5%	16.6%	50%	83.3%	95%
<b>climate sensitivities / K</b>	<b>ECS</b>	1.38	2.18	4.03	7.08	10.46	1.82	2.23	3.28	5.42	7.63
	<b>TCR</b>	0.85	1.25	2.17	3.06	3.37	1.21	1.40	1.73	2.18	2.59
<b>2019 ERF components / W m<sup>-2</sup></b>	<b>CO<sub>2</sub></b>	1.61	1.81	2.12	2.45	2.70	1.67	1.85	2.15	2.46	2.69
	<b>CH<sub>4</sub></b>	0.45	0.52	0.62	0.72	0.80	0.45	0.52	0.62	0.72	0.80
	<b>N<sub>2</sub>O</b>	0.16	0.17	0.20	0.22	0.24	0.16	0.17	0.20	0.22	0.24
	<b>other WMGHGs</b>	0.29	0.32	0.36	0.40	0.43	0.29	0.32	0.36	0.40	0.43
	<b>ozone</b>	0.23	0.33	0.47	0.61	0.70	0.23	0.33	0.47	0.61	0.70
	<b>stratospheric H<sub>2</sub>O from CH<sub>4</sub></b>	0.01	0.03	0.05	0.07	0.09	0.01	0.03	0.05	0.07	0.09
	<b>aerosol-radiation interaction</b>	-0.60	-0.47	-0.30	-0.15	-0.03	-0.59	-0.46	-0.31	-0.16	-0.05
	<b>aerosol-cloud interaction</b>	-2.28	-1.48	-0.70	-0.26	-0.05	-1.19	-0.90	-0.53	-0.24	-0.07
	<b>total aerosol</b>	-2.63	-1.81	-1.02	-0.53	-0.27	-1.51	-1.23	-0.85	-0.53	-0.32
	<b>black carbon on snow</b>	0.04	0.06	0.09	0.14	0.19	0.04	0.06	0.09	0.14	0.19
<b>anthropogenic</b>	<b>contrails</b>	0.01	0.03	0.06	0.08	0.10	0.01	0.03	0.06	0.08	0.10
	<b>albedo from land use change</b>	-0.35	-0.29	-0.20	-0.11	-0.05	-0.35	-0.29	-0.20	-0.11	-0.05
	<b>total anthropogenic</b>	1.01	1.86	2.73	3.39	3.82	2.16	2.47	2.93	3.40	3.73

### 4.3.5 Sensitivity to observational dataset

As stated in Section 4.1, the choice of observational dataset used in the Global Warming Index calculation may project significantly onto our results. Here we carry out an identical constraining procedure to that described in Section 4.3, but with the distribution of present-day level / rate calculated for each observational product in turn. Constrained values of the ECS,

620 TCR and projected 2100 warming under an SSP2-45 pathway are shown in Table 9. This sensitivity analysis demonstrates how important the chosen observational dataset is: projections under an SSP2-45 pathway can vary by over 0.2 K depending on the dataset used to determine the constraint.

**Table 9.** Sensitivity of results for the key metrics to the choice of observational dataset used in the Global Warming Index calculation.

quantity percentile dataset	ECS / K					TCR / K					2100 warming relative to 1995-2014 / K				
	5%	16.6%	50%	83.3%	95%	5%	16.6%	50%	83.3%	95%	5%	16.6%	50%	83.3%	95%
<b>HadCRUT5</b>	2.03	2.45	3.35	4.90	6.78	1.37	1.54	1.84	2.21	2.50	1.28	1.53	2.00	2.64	3.20
<b>HadCRUT4</b>	1.80	2.19	3.03	4.45	6.18	1.21	1.38	1.67	2.02	2.32	1.12	1.35	1.79	2.39	2.93
<b>NOAA</b>	1.97	2.38	3.25	4.77	6.61	1.32	1.50	1.80	2.15	2.43	1.24	1.49	1.95	2.56	3.10
<b>GISTEMP</b>	1.99	2.41	3.30	4.81	6.63	1.34	1.52	1.81	2.17	2.46	1.26	1.51	1.97	2.59	3.14
<b>CW</b>	1.89	2.29	3.16	4.63	6.42	1.27	1.44	1.74	2.10	2.40	1.18	1.42	1.88	2.49	3.04
<b>BERKELEY</b>	2.01	2.43	3.33	4.88	6.73	1.36	1.53	1.83	2.20	2.48	1.27	1.52	1.99	2.62	3.18

#### 4.4 Constrained idealised experiments

Here we carry out standard CMIP6 experiments used in diagnosing the key properties of the climate - the abrupt-4xCO<sub>2</sub> and 1pctCO<sub>2</sub> experiments - with the FULL and CONSTRAINED parameter ensembles. This represents a test of whether our parameter sampling methods are sufficient to ensure that the range of carbon cycle and climate system responses are sampled from (as informed by the CMIP6 ensemble). We see in [fig-Figure 8a, b](#) that the FULL 90% credible interval ~~elosely matches spans~~ the CMIP6 model ensemble range. ~~The most significant discrepancy between the FULL ensemble and the CMIP6 model ensemble is apparent in figures 8d, e, f; the FULL ensemble carbon cycle does not completely span the range of 11 C4MIP models, particularly at the high end of airborne fraction.~~ This occurs due to the use of a lower central  $r_0$  value, ~~consistent with historical observations, in the FULL parameter sample, rather than taking the central value as the mean of the C4MIP model tunings,~~ though with a longer lower tail. The FULL ensemble ~~does span~~ also spans the range of carbon-cycle ~~radiation feedback behaviour found in the behaviour in 11 C4MIP models (2, fig 8g)~~ on decadal timescales in Figures 8d, e, f, including radiation feedbacks (K. Arora et al., 2020, Figure 8g). The CONSTRAINED ensemble, as expected from the climate sensitivity results ~~above~~ in Section 4.3, is significantly less spread than the CMIP6 model ensemble. It precludes both models with high and low climate sensitivities. Although our constraint does not significantly affect the carbon-cycle parameters, it does preclude some FULL ensemble members with a high airborne fraction, more apparent towards the end of the experiments. The CONSTRAINED ensemble implies a likely range ([fig-Figure 8c](#)) for the (CO<sub>2</sub>-only) TCRE (Matthews et al., 2009; Allen et al., 2009; Zickfeld et al., 2016; MacDougall, 2016) of ~~1.17~~~~1.27~~ - ~~1.84~~~~1.85~~, with a central estimate of ~~1.45~~  
~~1.53~~ and 5-95% range of ~~1.00~~~~1.11~~ - ~~2.13~~~~2.12~~ K TtC<sup>-1</sup>, based on the temperature response at a cumulative CO<sub>2</sub> emission of 1000 GtC. ~~If instead we estimate the TCRE at a cumulative emission of 3000 GtC, this estimate is reduced by around 12% due to the~~ The slight non-linearity in the temperature–cumulative emission relationship results in the best-estimate instantaneous TCRE reducing by around 15 % per additional 1000 GtC. These estimates are consistent with recent estimates based on the observational record (Millar and Friedlingstein, 2018; Gillett et al., 2013); though our best-estimate is slightly higher and the range less spread. This tighter range may be due to the noise reduction from using an idealised experiment and model with no representation of internal variability. It is important to note that our TCRE estimates hold the same sensitivity to the choice of observational dataset used in the Global Warming Index calculation as the TCR (Table 9).

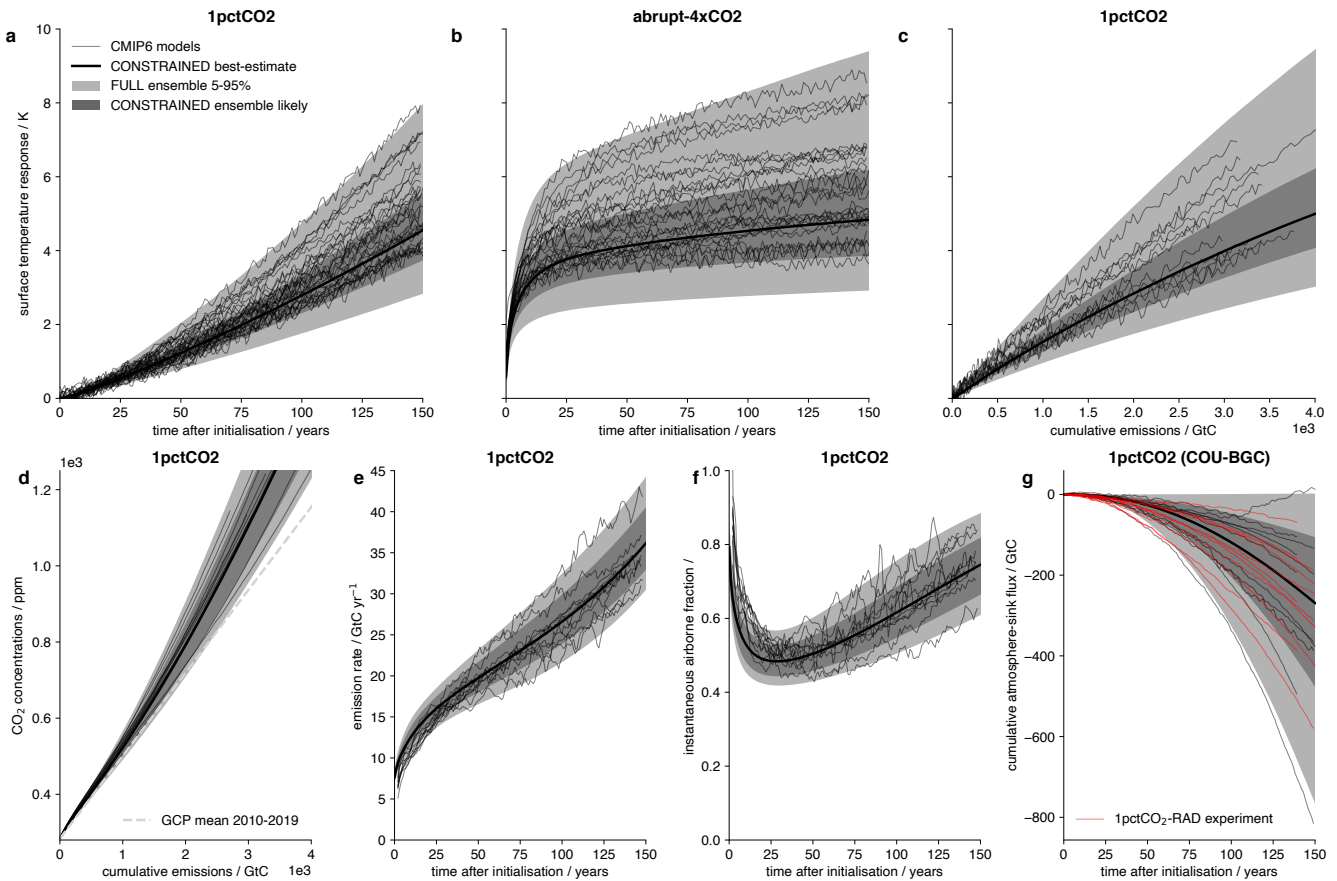


**Figure 8.** Idealised CMIP6 experiments with FULL and CONSTRAINED FaIRv2.0.0-alpha ensembles. Thin black lines show drift-corrected CMIP6 model data. Light-grey shading indicates FULL ensemble 5-95 % range. Dark-grey shading indicates CONSTRAINED ensemble likely (17-83 %) range. Thick black line shows central CONSTRAINED series. Dashed grey line in d shows airborne fraction for the most recent decade estimated from the most recent Global Carbon Project data (Friedlingstein et al., 2019) Budget (Friedlingstein et al., 2020), calculated by dividing the atmospheric carbon flux by the mean CO<sub>2</sub> emission rate over this period (see Friedlingstein et al. Figure 9). Thin red lines in g show data directly from the radiatively-coupled C4MIP experiment, while thin black lines show an estimate of the radiation feedback on carbon sink strength as the difference between the fully- and biogeochemically-coupled C4MIP experiments.

## 4.5 Constrained scenario projections

We use our CONSTRAINED parameter ensemble to project end-of-century warming and ERF in FaIRv2.0. Taking CO<sub>2</sub>

emissions until 2014 from the Global Carbon Project (Friedlingstein et al., 2019), all other emissions from the RCMIP protocol, and land-use change and natural ERF timeseries from the SSP ERF timeseries database (Smith, 2020), we run both the FULL and CONSTRAINED ensembles for each SSP (Riahi et al., 2017). The FULL ensemble should not be used for projection and is included only to demonstrate the impact of the constraint. 2100 warming relative to 1861–1880 / K 5.17 5.0 8.3 9.5 5.17 5.0  
8.3 9.5 ssp119 0.749 1.02 1.49 2.10 2.67 0.848 1.00 1.27 1.63 1.96 ssp126 0.984 1.33 1.92 2.65 3.32 1.100 1.29 1.63 2.05  
2.44 ssp245 1.550 2.08 2.97 4.03 4.93 1.800 2.08 2.56 3.12 3.60 ssp370 2.150 2.91 4.18 5.65 6.84 2.720 3.08 3.67 4.31 4.81  
ssp370-lowNTCF-aerchemmip 2.460 3.25 4.53 6.01 7.19 2.790 3.20 3.89 4.67 5.29 ssp370-lowNTCF-gidden 2.060 2.74 3.86  
5.17 6.23 2.370 2.72 3.32 4.01 4.55 ssp434 1.150 1.55 2.24 3.10 3.87 1.360 1.57 1.93 2.38 2.78 ssp460 1.790 2.39 3.39 4.57  
5.56 2.100 2.41 2.93 3.53 4.02 ssp534-over 1.140 1.54 2.24 3.14 3.96 1.280 1.50 1.90 2.41 2.88 ssp585 2.880 3.80 5.29 6.99  
8.33 3.250 3.73 4.54 5.46 6.18 2100 anthropogenic ERF / W m<sup>-2</sup> ssp119 1.700 1.89 2.16 2.45 2.67 1.760 1.93 2.18 2.45  
2.64 ssp126 2.260 2.50 2.85 3.22 3.50 2.330 2.55 2.87 3.20 3.45 ssp245 3.710 4.14 4.73 5.33 5.79 3.960 4.30 4.80 5.33 5.71  
ssp370 5.240 6.10 7.18 8.20 8.92 6.020 6.55 7.34 8.16 8.75 ssp370-lowNTCF-aerchemmip 6.190 6.79 7.65 8.53 9.19 6.440  
6.97 7.74 8.54 9.11 ssp370-lowNTCF-gidden 5.120 5.70 6.54 7.40 8.05 5.380 5.88 6.63 7.39 7.95 ssp434 2.640 2.96 3.41 3.86  
4.21 2.850 3.10 3.46 3.85 4.13 .0 for each SSP (Riahi et al., 2017). In Figures 9 & 10 we also compare our CONSTRAINED FaIRv2.0.0 projections to the default setup of MAGICC7.1.0-beta. The two models exhibit some notable differences, particularly in radiative forcing projections due to aerosol emissions and ozone concentrations. For a complete comparison of the CONSTRAINED ensemble with the probabilistic setup of MAGICC7, see Nicholls et al. (2021).

ssp460 4.320 4.80 5.48 6.18 6.69 4.630 5.01 5.58 6.17 6.60

ssp534-over 2.500 2.78 3.19 3.64 3.99 2.590 2.85 3.22 3.62 3.92 The apparent slight warm bias at the present-day arises due to a combination of natural variability, in particular the so-called “hiatus” period (Trenberth and Fasullo, 2013), and a too-high response to natural forcings. As the CONSTRAINED ensemble is selected on the basis of the contributions of anthropogenic forcings to global warming only (via the anthropogenic warming index), any bias in the response to natural forcings will project onto the total temperature response. Although the estimated contribution of natural forcings to the present-day level of warming is observational dataset dependent, the mean contribution over all six datasets calculated within our global warming index methodology (ie. scaled by the optimal fingerprinting regression coefficients) is 0.03 K lower than within our CONSTRAINED ensemble relative to the 1850–1900 baseline period, suggesting that the climate response to natural forcings is slightly too high. This could be resolved by scaling the prescribed natural forcing data (Smith, 2020) by the average estimated optimal fingerprinting coefficient. However, we do not do this here, instead using the raw data for transparency. The selected 1850–1900 baseline period exacerbates this high response due to the significant volcanic activity during this period.

ssp585 7.260 7.95 8.95 9.97 10.70 7.530 8.15 9.06 10.00 10.70

680 The projections of future warming are comparable to other recent studies that have used various methodologies to constrain future warming (Brunner et al., 2020; Tokarska et al., 2020; Ribes et al., 2021). Overall, our central estimates agree very well

with Tokarska et al. (2020); Ribes et al. (2021), lying a little below those from Ribes et al. (2021). The lower quantiles of our projections generally lie between the estimates from Tokarska et al. (2020) and Ribes et al. (2021). Our upper quantiles (specifically 95 %) agree well with the estimates given in Ribes et al. (2021). Overall, we find that our projections are comparable to other recent studies, though in general a little less tightly constrained. Here we have used one relatively straightforward methodology to perform these constrained projections, but we expect that it would be possible to constrain these further through the use of more sophisticated methods or by adding in additional information to the constraint (such as the present level of CO<sub>2</sub> concentrations, or an estimate of the total ocean heat uptake - though this would require the energy balance model formulation of the FaIRv2.0.0 climate response to be used). A reasonable next step to improve the probabilistic projections from FaIRv2.0.0 might be to switch to a Markov chain Monte-Carlo approach, as used by other SCMs (Meinshausen et al., 2011b, 2019).

**Table 10.** Global warming and radiative forcing projections from the FaIRv2.0.0-alpha CONSTRAINED ensemble under the SSPs. Table S6 displays these warming projections relative to a pre-industrial baseline of 1850-1900.

	percentile	5%	16.6%	50%	83.3%	95%
2081-2100 warming relative to 1995-2014 / K	<b>ssp119</b>	0.16	0.30	0.57	0.96	1.33
	<b>ssp126</b>	0.45	0.63	0.95	1.41	1.83
	<b>ssp245</b>	1.18	1.42	1.85	2.42	2.91
	<b>ssp370</b>	2.01	2.29	2.76	3.37	3.88
	<b>ssp370-lowNTCF-aerchemmip</b>	2.03	2.35	2.93	3.67	4.31
	<b>ssp370-lowNTCF-gidden</b>	1.61	1.90	2.41	3.07	3.64
	<b>ssp434</b>	0.75	0.93	1.26	1.72	2.14
peak warming relative to 1995-2014 / K	<b>ssp460</b>	1.48	1.73	2.18	2.76	3.26
	<b>ssp534-over</b>	0.72	0.94	1.34	1.90	2.42
	<b>ssp585</b>	2.51	2.89	3.56	4.43	5.15
2100 anthropogenic ERF / W m <sup>-2</sup>	<b>ssp119</b>	0.44	0.54	0.76	1.08	1.41
	<b>ssp126</b>	0.57	0.72	1.02	1.46	1.88
	<b>ssp534-over</b>	1.08	1.29	1.67	2.17	2.63
	<b>ssp119</b>	1.86	2.05	2.34	2.65	2.89
	<b>ssp126</b>	2.45	2.70	3.07	3.48	3.80
	<b>ssp245</b>	4.20	4.58	5.16	5.79	6.25
	<b>ssp370</b>	6.38	6.97	7.85	8.75	9.42
	<b>ssp370-lowNTCF-aerchemmip</b>	6.69	7.27	8.13	9.02	9.67
	<b>ssp370-lowNTCF-gidden</b>	5.65	6.21	7.04	7.92	8.56
	<b>ssp434</b>	3.00	3.27	3.70	4.15	4.50
	<b>ssp460</b>	4.85	5.28	5.94	6.62	7.13
	<b>ssp534-over</b>	2.76	3.04	3.49	3.98	4.36
	<b>ssp585</b>	7.80	8.48	9.49	10.53	11.28

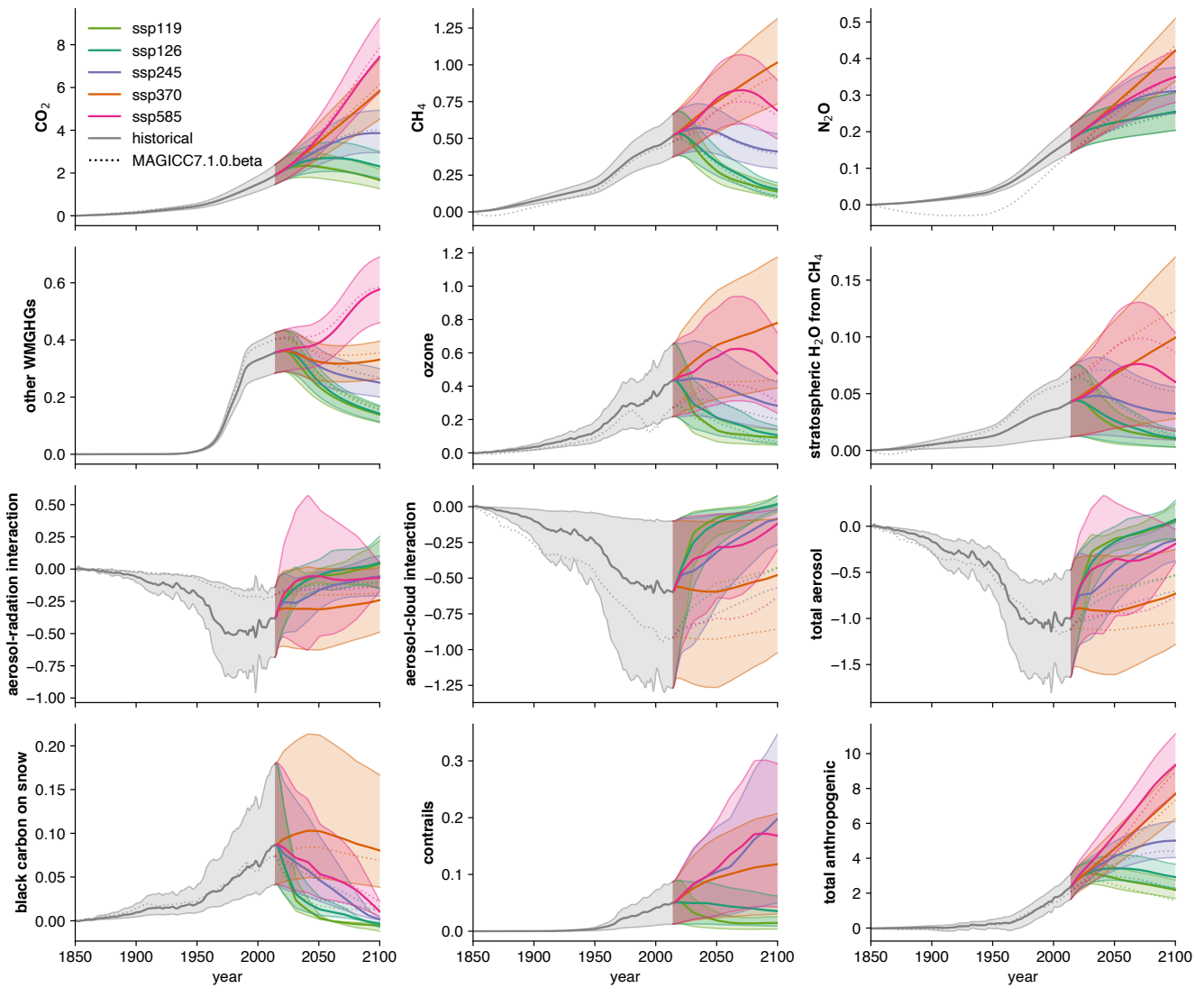


**Figure 9.** ERF timeseries in  $\text{W m}^{-2}$  by category for a range of SSP pathways using the [FaIRv2.0.0-alpha](#) CONSTRAINED parameter ensemble. Solid lines indicate central estimate and shading shows the 5-95% range. Dashed lines show default [projection](#) projections from a development version of the [MAGICC SCM](#) [MAGICC7.1.0-beta](#) from RCMIP (Nicholls et al., 2020a).

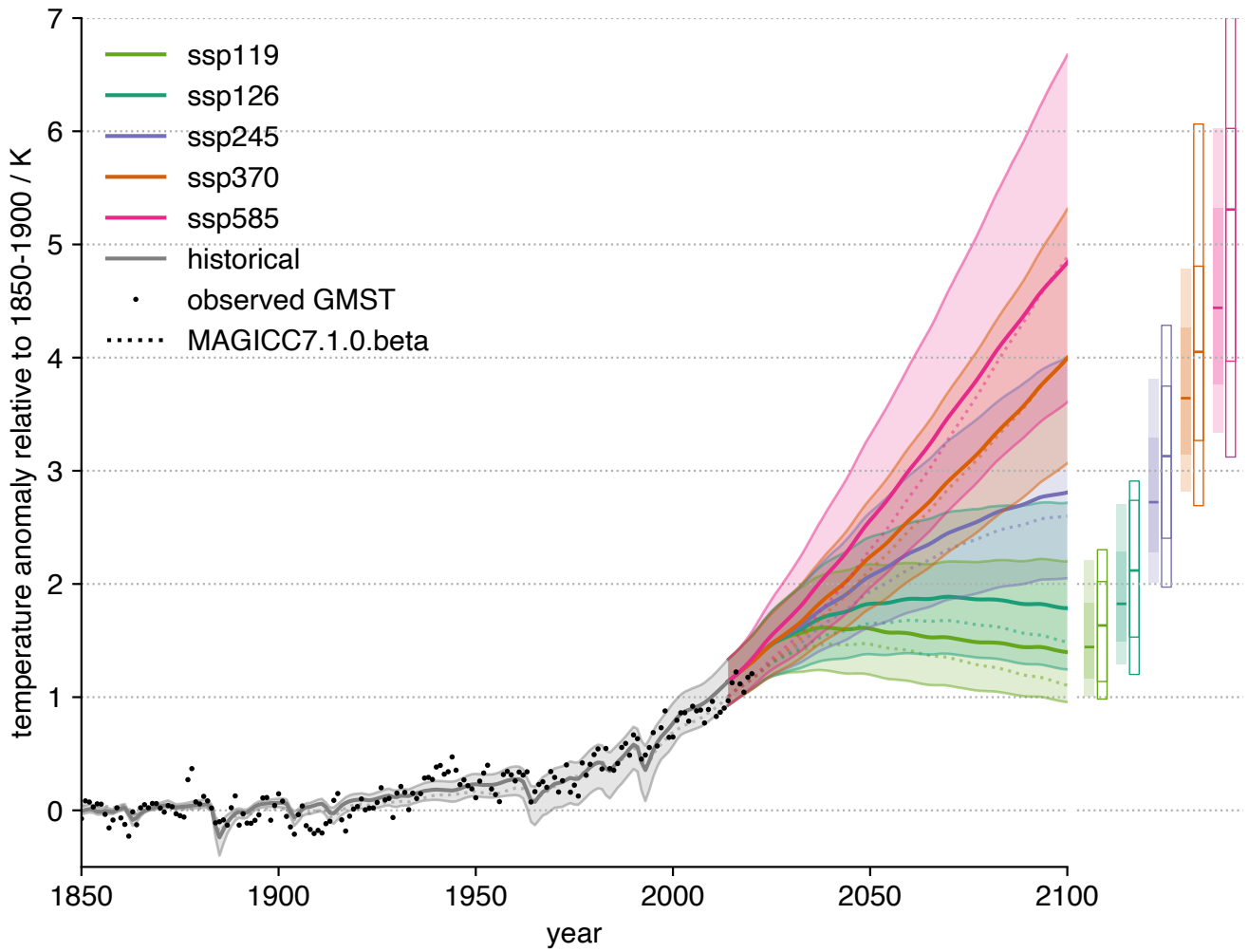


**Figure 10.** Surface temperature response projections for a range of SSPs with the [FaIRv2.0.0-alpha](#) CONSTRAINED parameter ensemble. Solid lines indicate central projection. Shading indicates a 5-95% range. Dashed line indicates default projection from [a development version of the MAGICC-SCM](#) [MAGICC7.1.0-beta](#) from RCMIP (Nicholls et al., 2020a). Dots show the mean of [5-6](#) observational datasets. Bars on the right-hand side of the figure show end-of-century (2081-2100) warming. Filled bars show CONSTRAINED best-estimate, and likely and 5-95% ranges. Unfilled bars show CMIP6 median, and likely and minimum–maximum range. The number of CMIP6 models used in each scenario is given in [table](#)-Table S4.

## 5 The response of simple climate models

The IPCC Special Report on 1.5°C warming (IPCC, 2018) included results from two SCMs, FaIRv1.3 (Smith et al., 2018) and MAGICC6 (Meinshausen et al., 2011a). One point of discussion following the report was the difference in results between these two models, with FaIRv1.3 tending to project a lower temperature response than MAGICC6 (Huppmann et al., 2018).

695 This has resulted in a widely-held belief that FaIRv1.3 is intrinsically “cooler” than MAGICC6 in general, a belief that some of these authors have unintentionally contributed to previously (Leach et al., 2018). This belief is unfounded: the response of an SCM is a function of the parameters used. Although some parameters may be chosen to be consistent with geophysical observation or theory, in general SCM parameters are tuned such that they emulate, or reproduce, either the output of more complex models, or observations of the Earth. Relating this to the models used in SR15, the FaIRv1.3 ensemble was tuned  
700 such that the model response lay within observed changes in global mean surface temperature since pre-industrial (Smith et al., 2018; Cowtan and Way, 2014); the MAGICC6 ensemble was constrained to observations up until 2009 (Meinshausen et al., 2009). The two different tuning targets naturally leads to differences in the response of FaIRv1.3 and MAGICC6. Here we emphasize that the differences between the models’ output is not systematic – it is the parameters used, and how these are selected (which is often a subjective decision on the part of the modellers), that determines the model response.

705

## 6 Uses of FaIRv2.0.0

We envisage that FaIRv2.0.0 will primarily be used for similar assessments as are carried out with ~~the current SCMs, such as providing probabilistic projections of atmospheric concentrations, radiative forcings and temperature anomalies for wide ranges of scenarios, such as in the SR15 scenario explorer (Huppmann et al., 2018). FaIRv2.0 could also easily be coupled to integrated assessment models (IAMs) to explore impacts of climate policy options~~ current SCMs. One advantage that FaIRv2.0.0 ~~has it~~ is that it was built with performance in mind, hence is easily vectorised. It can be vectorised in a programming language designed for array operations (such as Fortran, MATLAB, or the NumPy Python module) and hence FaIRv2.0.0 is extremely quick to run. For example, using ~~its present~~ the alpha Python implementation, FaIRv2.0.0 can compute  
715 the 1 million member FULL ensemble (emission driven for 52 gases, ~~78-81~~ forcing components, over the period 1750-2100) in under ~~30-40~~ minutes<sup>3</sup>. This speed provides significant advantages when computing large probabilistic ensembles, or when optimizing parameters. An important consideration for users computing probabilistic ensembles will be the memory required by FaIRv2.0.0 output, as this is more likely to be the limiting factor on a modern computer, rather than the model runtime. A related point is that the minimal equation set that FaIRv2.0.0 ~~can be run in programs for analysis of tabular data, including (but not limited to)~~ is composed of is easily transcribed into other programming languages. Although we would recommend  
720 using the official Python FaIR release<sup>4</sup> where possible, there are many cases where it might be required for FaIRv2.0.0 to be

<sup>3</sup>on a laptop with 31GB RAM and an Intel(R) Core(TM) i7-8750H@2.2GHz, 12 cores

<sup>4</sup><https://github.com/OMS-NetZero/FAIR>

converted into another language - such as GAMS, for use in integrated assessment models. We believe that the relative simplicity of FaIRv2.0.0 lends itself to this purpose. Of particular note is that FaIRv2.0.0, in its entirety, is able to be run in Excel. This opens up climate system exploration and experimentation to a large group of potential new users who are familiar with spreadsheets, but not formal scientific programming languages. ~~We suggest that the speed, simplicity and transparency~~ The user-base of Excel is estimated to be around 100 times larger than that of Python<sup>5</sup>. To aid with implementation in alternative languages where required, we have provided a brief set of notes on our own Python implementation of the development version of FaIRv2.0~~lends it to use in undergraduate and high school education in addition to scientific research. It can be used to explain (and demonstrate) important features of both the carbon (or other GHG) cycle and Earth's thermal response to radiative forcing, and is simple enough to use that students could themselves carry out experiments (such as a CO<sub>2</sub> doubling) easily with no prior experience and only basic computing skills.~~ 0 in the supplement.

In terms of possible academic uses of FaIRv2.0~~can also~~ 0, we have demonstrated two of the main ones: emulation of more complex models and probabilistic scenario projections. FaIRv2.0.0 can be used to rapidly investigate differences between ESMs, by tuning FaIRv2.0~~to emulate different full~~ 0 to emulate these complex models and comparing differences between the tuned parameter sets to identify which aspects of the models differ most, as was done with MAGICC in Meinshausen et al. (2011a, b). The ability to tune FaIRv2.0.0, as demonstrated here and in other work (Tsutsui, 2017; Joos et al., 2013; Millar et al., 2017), to more complex models also allows estimation of complex model response to a particular scenario or experiment without having to expend computer power to run the model itself; which could allow climate system uncertainties to be introduced more fully into integrated assessment studies by emulating the full CMIP6 ensemble within IAMs (providing some of the capability demonstrated by Meinshausen et al. (2011a) with a simpler model). The probabilistic scenario projection we demonstrated in Section 4 is a potentially more policy-relevant academic use of FaIRv2.0.0, since CMIP6 model emulations do not necessarily represent the best-estimate of some key properties of the real-life Earth system when historical observations are taken into account (Tokarska et al., 2020; Gillett et al., 2021). The speed of FaIRv2.0.0 allows very large parameter ensembles to be run rapidly, enabling all regions of plausible parameter space to be explored without requiring large quantities of computing resource. Although here we have performed one relatively simple methodology for the creation of an observationally constrained large ensemble, there are many possible ways to do this, for example using the Markov chain Monte-Carlo methods employed in several other SCMs (Nicholls et al., 2020b; Meinshausen et al., 2019, 2011b). A third academic use of FaIRv2.0.0, which we are interested in, is its incorporation into integrated assessment models (IAMs). Its simplicity and computational efficiency may make implementation within existing IAMs relatively more straightforward than for other SCMs, even if the whole model was required to be built up from scratch in whatever format would be required by the particular IAM.

Outside of academia, we propose that FaIRv2.0.0 could be used for emission climate impact accounting in industry. The UNFCCC standard for the reporting of greenhouse gas emissions is to account for emissions of all gases as a CO<sub>2</sub> equivalent quantity via the 100-year Global Warming Potential (GWP). However, GWPs do not adequately capture the behaviour

<sup>5</sup><https://info.cambridgespark.com/latest/python-vs-excel>

of short-lived climate pollutants such as methane (Cain et al., 2019), leading to the development of alternative metrics such as GWP\*. We suggest that such warming impacts could potentially instead be simulated using a simple climate model as an improvement upon the use of any of these metrics. Although this does represent a step-up in complexity, we believe that the relative simplicity of FaIRv2.0.0, when compared to other SCMs, makes it a strong candidate for this usage. In particular, the  
760 ability of FaIRv2.0.0 to be run in Excel could encourage this particular use-case. We suggest that the speed, simplicity and transparency of FaIRv2.0.0 also lends it to use in undergraduate and high-school education. It can be used to explain (and demonstrate) important features of both the carbon (or other GHG) cycle and Earth's thermal response to radiative forcing, and is simple enough to use that students could themselves carry out experiments (such as a CO<sub>2</sub> doubling) easily with no prior experience and only basic computing skills.

765

## 7 Conclusions

In this paper we have presented a significant update to the ~~FaIRv1.3~~ FaIR SCM (Smith et al., 2018), focussed on reducing the structural complexity of the model as much as possible. The updated model, FaIRv2.0.0, uses the five equations of the AR5  
770 impulse response model (Myhre et al., 2013) plus just one additional equation to allow the model to represent non-linearities in the carbon-cycle. We demonstrate that this reduction in complexity does not come at the cost of the model's ability to reproduce globally-averaged observations or output of more complex models from CMIP6 (Eyring et al., 2016). After demonstrating the ability of the model in emulating more complex models, we show how the model can be used for climate projection by constraining a large parameter ensemble.

775

There are many potential uses for FaIRv2.0.0 as a result of its simplicity and transparency. In addition to being available for the same probabilistic scenario assessment as is carried out by SCMs in reports such as SR15 (IPCC, 2018), it could be  
~~very easily~~ implemented into IAMs; and likely ~~improves~~ improve computational efficiency due to its vectorisation and resulting extremely rapid runtime. We encourage policy-makers to use FaIRv2.0.0 in order to directly assess whether warming  
780 implications are aligned with the intended outcomes of mitigation policies; since GHG accounting metrics used at present such as GWP do not provide accurate results for targets such as Net-Zero CO<sub>2</sub> due to the short life of some GHGs (Allen et al., 2018). To aid this use of FaIRv2.0.0, we will provide an Excel file containing the model with its default parameter set, ensuring FaIRv2.0~~as~~.0 is available for all interested parties, even those unfamiliar with computer programming languages. The Excel version of the model could also be used to assist teaching of climate change and climate processes; and could even allow students access to an easy-to-understand model that they could use themselves to explore future scenarios and the relative impacts  
785 of future emissions of different greenhouse gases; or demonstrate the importance of climate sensitivity in an interactive manner.

~~We aim to be able to provide complete gas-cycle parameter sets tuned to each of the CMIP6 ESMs in the near future, such~~

FaIRv2.0.0 sits at the very low end of complexity within the broad spectrum of currently available simple climate models.

790 It is a very highly parameterised model for simulating globally averaged relationships between greenhouse gas and aerosol emissions, atmospheric greenhouse gas concentrations, radiative forcing and surface temperature response. We have shown that despite its simplicity, it is able to span the wide range of behaviours exhibited by much more complex models, and that inferred from observations. In addition, we have provided some basic comparisons to both the previous version of FaIR(v1.5), and the widely used MAGICC SCM (Meinshausen et al., 2011a, b, 2019). More detailed comparisons are outside the remit  
795 of this paper, but RCMIP (Nicholls et al., 2020b, a) covers this topic comprehensively. We expect that FaIRv2.0 is able to be used to emulate the full CMIP6 ensemble and to improve understanding of how these models differ in a single consistent framework. We hope that such parameter sets may also provide users in other related fields, such as climate policy, who do not have experience with climate models, access to a robust emulation of complex climate models with little learning curve.  
800 0 is very close to as simple as an SCM could get without losing a significant proportion of this representation ability. However, it does not explicitly simulate the physical processes behind these variables, which may preclude it from some applications where other, more complex SCMs such as MAGICC would be usable. Overall, however, we hope that FaIRv2.0.0 will be an important contribution to the available set of SCMs given its wide range of potential use-cases and may open up climate system modelling to a wide range of novel users in both industry and education.

805 *Code and data availability.* FaIRv2.0.0-alpha code and the code used to produce the figures is publicly available at TODO. All data used in this study is publicly available at the relevant cited sources.

*Author contributions.* NJL, SJ and MRA conceived the study. NJL and SJ wrote the model code. NJL tuned the model to CMIP6 data and carried out the constrained ensemble. BW and TW assisted with tuning model parameters. CJS provided CMIP6 aerosol forcing data from RFMIP and advised on the forcing component parameterisations. JT advised on the thermal response component. JL and MC advised on model uses and tested the model. NJL produced the figures. NJL, CJS, ZN, SJ, JL and MRA wrote the manuscript.

810 *Competing interests.* The authors declare that they have no competing interests.

*Acknowledgements.* We acknowledge the World Climate Research Programme, which, through its Working Group on Coupled Modelling, coordinated and promoted both CMIP5 and CMIP6.

## References

- J.B. Burkholder (lead author), Ø. Hodnebrog and V.L. Orkin, Appendix A: Summary of Abundances, Lifetimes, ODPs, REs, GWPs, and  
815 GTPs, Scientific Assessment of Ozone Depletion: 2018, Global Ozone Research and Monitoring Project – Report No. 58, World Meteorological Organization, Geneva, Switzerland, 2018.
- Alexander, K. and Easterbrook, S. M.: The software architecture of climate models: a graphical comparison of CMIP5 and EMICAR5 configurations, *Geosci. Model Dev.*, 8, 1221–1232, <https://doi.org/10.5194/gmd-8-1221-2015>, 2015.
- Allen, M. R., Frame, D. J., Huntingford, C., Jones, C. D., Lowe, J. A., Meinshausen, M., and Meinshausen, N.: Warming caused by cumulative  
820 carbon emissions towards the trillionth tonne, *Nature*, 458, 1163–1166, <https://doi.org/10.1038/nature08019>, 2009.
- Allen, M. R., Shine, K. P., Fuglestvedt, J. S., Millar, R. J., Cain, M., Frame, D. J., and Macey, A. H.: A solution to the misrepresentations of CO<sub>2</sub>-equivalent emissions of short-lived climate pollutants under ambitious mitigation, *npj Climate and Atmospheric Science*, 1,  
825 <https://doi.org/10.1038/s41612-018-0026-8>, 2018.
- Bellouin, N., Davies, W., Shine, K. P., Quaas, J., Mülmenstädt, J., Forster, P. M., Smith, C., Lee, L., Regayre, L., Brasseur, G., Sudarchikova,  
830 N., Bouarar, I., Boucher, O., and Myhre, G.: Radiative forcing of climate change from the Copernicus reanalysis of atmospheric composition, *Earth System Science Data*, 12, 1649–1677, <https://doi.org/10.5194/essd-12-1649-2020>, 2020a.
- Bellouin, N., Quaas, J., Gryspeerdt, E., Kinne, S., Stier, P., Watson-Parris, D., Boucher, O., Carslaw, K. S., Christensen, M., Daniau, A. L.,  
835 Dufresne, J. L., Feingold, G., Fiedler, S., Forster, P., Gettelman, A., Haywood, J. M., Lohmann, U., Malavelle, F., Mauritzen, T., McCoy, D. T., Myhre, G., Mülmenstädt, J., Neubauer, D., Possner, A., Rugenstein, M., Sato, Y., Schulz, M., Schwartz, S. E., Sourdeval, O., Storelvmo, T., Toll, V., Winker, D., and Stevens, B.: Bounding Global Aerosol Radiative Forcing of Climate Change, Tech. Rep. 1,  
840 <https://doi.org/10.1029/2019RG000660>, 2020b.
- Bodman, R. W. and Jones, R. N.: Bayesian estimation of climate sensitivity using observationally constrained simple climate models, *Wiley Interdisciplinary Reviews: Climate Change*, 7, 461–473, <https://doi.org/10.1002/wcc.397>, 2016.
- Bond, T. C., Doherty, S. J., Fahey, D. W., Forster, P. M., Berntsen, T., Deangelo, B. J., Flanner, M. G., Ghan, S., Kärcher, B., Koch, D.,  
845 Kinne, S., Kondo, Y., Quinn, P. K., Sarofim, M. C., Schultz, M. G., Schulz, M., Venkataraman, C., Zhang, H., Zhang, S., Bellouin, N., Guttikunda, S. K., Hopke, P. K., Jacobson, M. Z., Kaiser, J. W., Klimont, Z., Lohmann, U., Schwarz, J. P., Shindell, D., Storelvmo, T., Warren, S. G., and Zender, C. S.: Bounding the role of black carbon in the climate system: A scientific assessment, *Journal of Geophysical Research Atmospheres*, 118, 5380–5552, <https://doi.org/10.1002/jgrd.50171>, 2013.
- Brunner, L., Pendergrass, A. G., Lehner, F., Merrifield, A. L., Lorenz, R., and Knutti, R.: Reduced global warming from CMIP6 projections  
850 when weighting models by performance and independence, *Earth System Dynamics*, 11, 995–1012, <https://doi.org/10.5194/esd-11-995-2020>, 2020.
- Butchart, N. and Scaife, A. A.: Removal of chlorofluorocarbons by increased mass exchange between the stratosphere and troposphere in a changing climate, *Nature*, 410, 799–802, <https://doi.org/10.1038/35071047>, 2001.
- Cain, M., Lynch, J., Allen, M. R., Fuglestvedt, J. S., Frame, D. J., and Macey, A. H.: Improved calculation of warming-equivalent emissions  
855 for short-lived climate pollutants, *npj Climate and Atmospheric Science*, 2, 29, <https://doi.org/10.1038/s41612-019-0086-4>, 2019.
- Cinquini, L., Crichton, D., Mattmann, C., Harney, J., Shipman, G., Wang, F., Ananthakrishnan, R., Miller, N., Denvil, S., Morgan, M., Pobre, Z., Bell, G. M., Doutiaux, C., Drach, R., Williams, D., Kershaw, P., Pascoe, S., Gonzalez, E., Fiore, S., and Schweitzer, R.: The Earth System Grid Federation: An open infrastructure for access to distributed geospatial data, *Future Generation Computer Systems*, 36, 400–417, <https://doi.org/10.1016/j.future.2013.07.002>, 2014.

- 850 Collins, M., Knutti, R., Arblaster, J., Dufresne, J.-L., Fichefet, T., Friedlingstein, P., Gao, X., Gutowski, W. J., Johns, T., Krinner, G., Shongwe, M., Tebaldi, C., Weaver, A. J., and Wehner, M.: Long-term Climate Change: Projections, Commitments and Irreversibility, in: Climate Change 2013: The Physical Science Basis. Contribution of Working Group I to the Fifth Assessment Report of the Intergovernmental Panel on Climate Change, edited by Stocker, T. F., Qin, D., Plattner, G.-K., Tignor, M., Allen, S. K., Boschung, J., Nauels, A., Xia, Y., Bex, V., and Midgley, P. M., chap. 12, pp. 1029–1136, Cambridge University Press, Cambridge, United Kingdom and New York, NY, USA, <https://doi.org/10.1017/CBO9781107415324.024>, 2013.
- 855 Cowtan, K. and Way, R. G.: Coverage bias in the HadCRUT4 temperature series and its impact on recent temperature trends, Quarterly Journal of the Royal Meteorological Society, 140, 1935–1944, <https://doi.org/10.1002/qj.2297>, 2014.
- Cummins, D. P., Stephenson, D. B., and Stott, P. A.: Optimal estimation of stochastic energy balance model parameters, Journal of Climate, 33, 7909–7926, <https://doi.org/10.1175/JCLI-D-19-0589.1>, 2020.
- 860 Engel, A., Rigby, M., Burkholder, J., Fernandez, R., Froidevaux, L., Hall, B., Hossaini, R., Saito, T., Vollmer, M., and Yao, B.: Update on Ozone-Depleting Substances (ODSs) and Other Gases of Interest to the Montreal Protocol, Chapter 1 in Scientific Assessment of Ozone Depletion: 2018, Global Ozone Research and Monitoring Project — Report No. 58, World Meteorological Organization, Geneva, Switzerland, 2018.
- Etminan, M., Myhre, G., Highwood, E. J., and Shine, K. P.: Radiative forcing of carbon dioxide, methane, and nitrous oxide: A significant revision of the methane radiative forcing, Geophysical Research Letters, 43, 12,614–12,623, <https://doi.org/10.1002/2016GL071930>, 2016.
- 865 Eyring, V., Bony, S., Meehl, G. A., Senior, C. A., Stevens, B., Stouffer, R. J., and Taylor, K. E.: Overview of the Coupled Model Intercomparison Project Phase 6 (CMIP6) experimental design and organization, Geoscientific Model Development, 9, 1937–1958, <https://doi.org/10.5194/gmd-9-1937-2016>, 2016.
- 870 Forest, C. E., Stone, P. H., Sokolov, A. P., Allen, M. R., and Webster, M. D.: Quantifying uncertainties in climate system properties with the use of recent climate observations, Science, 295, 113–117, <https://doi.org/10.1126/science.1064419>, 2002.
- Friedlingstein, P., Jones, M. W., O’Sullivan, M., Andrew, R. M., Hauck, J., Peters, G. P., Peters, W., Pongratz, J., Sitch, S., Le Quéré, C., DBakker, O. C., Canadell, J. G., Ciais, P., Jackson, R. B., Anthoni, P., Barbero, L., Bastos, A., Bastrikov, V., Becker, M., Bopp, L., Buitenhuis, E., Chandra, N., Chevallier, F., Chini, L. P., Currie, K. I., Feely, R. A., Gehlen, M., Gilfillan, D., Gkrizalis, T., Goll, D. S., Gruber, N., Gutekunst, S., Harris, I., Haverd, V., Houghton, R. A., Hurtt, G., Ilyina, T., Jain, A. K., Joetzjer, E., Kaplan, J. O., Kato, E., Goldewijk, K. K., Korsbakken, J. I., Landschützer, P., Lauvset, S. K., Lefèvre, N., Lenton, A., Lienert, S., Lombardozzi, D., Marland, G., McGuire, P. C., Melton, J. R., Metzl, N., Munro, D. R., Nabel, J. E., Nakaoka, S. I., Neill, C., Omar, A. M., Ono, T., Peregon, A., Pierrot, D., Poulter, B., Rehder, G., Resplandy, L., Robertson, E., Rödenbeck, C., Séférian, R., Schwinger, J., Smith, N., Tans, P. P., Tian, H., Tilbrook, B., Tubiello, F. N., Van Der Werf, G. R., Wiltshire, A. J., and Zaehle, S.: Global carbon budget 2019, Earth System Science Data, 11, 1783–1838, <https://doi.org/10.5194/essd-11-1783-2019>, 2019.
- 880 Friedlingstein, P., O’Sullivan, M., Jones, M. W., Andrew, R. M., Hauck, J., Olsen, A., Peters, G. P., Peters, W., Pongratz, J., Sitch, S., Le Quéré, C., Canadell, J. G., Ciais, P., Jackson, R. B., Alin, S., Aragão, L. E. O. C., Arneth, A., Arora, V., Bates, N. R., Becker, M., Benoit-Cattin, A., Bittig, H. C., Bopp, L., Bultan, S., Chandra, N., Chevallier, F., Chini, L. P., Evans, W., Florentie, L., Forster, P. M., Gasser, T., Gehlen, M., Gilfillan, D., Gkrizalis, T., Gregor, L., Gruber, N., Harris, I., Hartung, K., Haverd, V., Houghton, R. A., Ilyina, T., Jain, A. K., Joetzjer, E., Kadono, K., Kato, E., Kitidis, V., Korsbakken, J. I., Landschützer, P., Lefèvre, N., Lenton, A., Lienert, S., Liu, Z., Lombardozzi, D., Marland, G., Metzl, N., Munro, D. R., Nabel, J. E. M. S., Nakaoka, S.-I., Niwa, Y., O’Brien, K., Ono, T., Palmer, P. I., Pierrot, D., Poulter, B., Resplandy, L., Robertson, E., Rödenbeck, C., Schwinger, J., Séférian, R., Skjelvan, I., Smith, A. J. P.,

- Sutton, A. J., Tanhua, T., Tans, P. P., Tian, H., Tilbrook, B., van der Werf, G., Vuichard, N., Walker, A. P., Wanninkhof, R., Watson, A. J., Willis, D., Wiltshire, A. J., Yuan, W., Yue, X., and Zaehle, S.: Global Carbon Budget 2020, *Earth System Science Data*, 12, 3269–3340, 890 <https://doi.org/10.5194/essd-12-3269-2020>, 2020.
- Geoffroy, O., Saint-Martin, D., Olivié, D. J. L., Volodire, A., Bellon, G., Tytéca, S., Geoffroy, O., Saint-Martin, D., Olivié, D. J. L., Volodire, A., Bellon, G., and Tytéca, S.: Transient Climate Response in a Two-Layer Energy-Balance Model. Part I: Analytical Solution and Parameter Calibration Using CMIP5 AOGCM Experiments, *Journal of Climate*, 26, 1841–1857, <https://doi.org/10.1175/JCLI-D-12-00195.1>, 2013.
- Gillett, N. P., Arora, V. K., Matthews, D., Allen, M. R., Gillett, N. P., Arora, V. K., Matthews, D., and Allen, M. R.: Constraining the Ratio of Global Warming to Cumulative CO <sub>2</sub> Emissions Using CMIP5 Simulations\*, *Journal of Climate*, 26, 6844–6858, 895 <https://doi.org/10.1175/JCLI-D-12-00476.1>, 2013.
- Gillett, N. P., Kirchmeier-Young, M., Ribes, A., Shiogama, H., Hegerl, G. C., Knutti, R., Gastineau, G., John, J. G., Li, L., Nazarenko, L., Rosenbloom, N., Selander, Ø., Wu, T., Yukimoto, S., and Ziehn, T.: Constraining human contributions to observed warming since the 900 pre-industrial period, *Nature Climate Change*, pp. 1–6, <https://doi.org/10.1038/s41558-020-00965-9>, 2021.
- Goodwin, P., Williams, R. G., Roussenov, V. M., and Katavouta, A.: Climate Sensitivity From Both Physical and Carbon Cycle Feedbacks, *Geophysical Research Letters*, 46, 7554–7564, <https://doi.org/10.1029/2019GL082887>, 2019.
- Gregory, J. M., Ingram, W. J., Palmer, M. A., Jones, G. S., Stott, P. A., Thorpe, R. B., Lowe, J. A., Johns, T. C., and Williams, K. D.: A new method for diagnosing radiative forcing and climate sensitivity, *Geophysical Research Letters*, 31, <https://doi.org/10.1029/2003GL018747>, 905 2004.
- Haustein, K., Allen, M. R., Forster, P. M., Otto, F. E. L., Mitchell, D. M., Matthews, H. D., and Frame, D. J.: A real-time Global Warming Index, *Scientific Reports*, 7, 15 417, <https://doi.org/10.1038/s41598-017-14828-5>, 2017.
- Held, I. M., Winton, M., Takahashi, K., Delworth, T., Zeng, F., Vallis, G. K., Held, I. M., Winton, M., Takahashi, K., Delworth, T., Zeng, F., and Vallis, G. K.: Probing the Fast and Slow Components of Global Warming by Returning Abruptly to Preindustrial Forcing, *Journal of Climate*, 23, 2418–2427, <https://doi.org/10.1175/2009JCLI3466.1>, 2010.
- Hersbach, H., Bell, B., Berrisford, P., Hirahara, S., Horányi, A., Muñoz-Sabater, J., Nicolas, J., Peubey, C., Radu, R., Schepers, D., Simmons, A., Soci, C., Abdalla, S., Abellán, X., Balsamo, G., Bechtold, P., Biavati, G., Bidlot, J., Bonavita, M., De Chiara, G., Dahlgren, P., Dee, D., Diamantakis, M., Dragani, R., Flemming, J., Forbes, R., Fuentes, M., Geer, A., Haimberger, L., Healy, S., Hogan, R. J., Hölm, E., Janisková, M., Keeley, S., Laloyaux, P., Lopez, P., Lupu, C., Radnoti, G., de Rosnay, P., Rozum, I., Vamborg, F., Vil-910 laume, S., and Thépaut, J. N.: The ERA5 global reanalysis, *Quarterly Journal of the Royal Meteorological Society*, 146, 1999–2049, <https://doi.org/10.1002/qj.3803>, 2020.
- Hoesly, R. M., Smith, S. J., Feng, L., Klimont, Z., Janssens-Maenhout, G., Pitkanen, T., Seibert, J. J., Vu, L., Andres, R. J., Bolt, R. M., Bond, T. C., Dawidowski, L., Kholod, N., Kurokawa, J.-i., Li, M., Liu, L., Lu, Z., Moura, M. C. P., O'Rourke, P. R., and Zhang, Q.: Historical (1750–2014) anthropogenic emissions of reactive gases and aerosols from the Community Emissions Data System (CEDS), *Geoscientific Model Development*, 11, 369–408, <https://doi.org/10.5194/gmd-11-369-2018>, 2018.
- Holmes, C. D., Prather, M. J., Søvde, O. A., and Myhre, G.: Future methane, hydroxyl, and their uncertainties: key climate and emission parameters for future predictions, *Atmospheric Chemistry and Physics*, 13, 285–302, <https://doi.org/10.5194/acp-13-285-2013>, 2013.
- Hooss, G., Voss, R., Hasselmann, K., Maier-Reimer, E., and Joos, F.: A nonlinear impulse response model of the coupled carbon cycle-climate system (NICCS), *Climate Dynamics*, 18, 189–202, <https://doi.org/10.1007/s003820100170>, 2001.

- 925 Huppmann, D., Kriegler, E., Krey, V., Riahi, K., Rogelj, J., Rose, S. K., Weyant, J., Bauer, N., Bertram, C., Bosetti, V., Calvin, K., Doelman, J.,  
Drouet, L., Emmerling, J., Frank, S., Fujimori, S., Gernaat, D., Grubler, A., Guiavarch, C., Haigh, M., Holz, C., Iyer, G., Kato, E., Keramidas, K., Kitous, A., Leblanc, F., Liu, J.-Y., Löffler, K., Luderer, G., Marcucci, A., McCollum, D., Mima, S., Popp, A., Sands, R. D., Sano, F.,  
Strefler, J., Tsutsui, J., Van Vuuren, D., Vrontisi, Z., Wise, M., and Zhang, R.: IAMC 1.5°C Scenario Explorer and Data hosted by IIASA,  
930 Integrated Assessment Modeling Consortium & International Institute for Applied Systems Analysis, <https://doi.org/10.22022/SR15/08-2018.15429>, 2018.
- IPCC: Global warming of 1.5°C. An IPCC Special Report on the impacts of global warming of 1.5°C above pre-industrial levels and related  
global greenhouse gas emission pathways, in the context of strengthening the global response to the threat of climate change,, 2018.
- 935 IPCC, Prather, M., Flato, G., Friedlingstein, P., Jones, C., Lamarque, J.-F., Liao, H., and Rasch, P.: Annex II: Climate System Scenario  
Tables , in: Climate Change 2013: The Physical Science Basis. Contribution of Working Group I to the Fifth Assessment Report of the  
Intergovernmental Panel on Climate Change, edited by Stocker, T. F., Qin, D., Plattner, G.-K., Tignor, M., Allen, S. K., Boschung, J.,  
Nauels, A., Xia, Y., Bex, V., and Midgley, P. M., chap. AII, pp. 1395–1446, Cambridge University Press, Cambridge, United Kingdom  
and New York, NY, USA, <https://doi.org/10.1017/CBO9781107415324.030>, 2013.
- Jenkins, S., Millar, R. J., Leach, N., and Allen, M. R.: Framing Climate Goals in Terms of Cumulative CO2-Forcing-Equivalent Emissions,  
Geophysical Research Letters, 45, 2795– 2804, <https://doi.org/10.1002/2017GL076173>, 2018.
- 940 Jiménez-de-la Cuesta, D. and Mauritsen, T.: Emergent constraints on Earth’s transient and equilibrium response to doubled CO2 from post-  
1970s global warming, Nature Geoscience, <https://doi.org/10.1038/s41561-019-0463-y>, 2019.
- Jones, C. D., Arora, V., Friedlingstein, P., Bopp, L., Brovkin, V., Dunne, J., Graven, H., Hoffman, F., Ilyina, T., John, J. G.,  
Jung, M., Kawamiya, M., Koven, C., Pongratz, J., Raddatz, T., Randerson, J. T., and Zaehle, S.: C4MIP – The Coupled Climate–Carbon Cycle Model Intercomparison Project: experimental protocol for CMIP6, Geoscientific Model Development, 9, 2853–2880,  
945 <https://doi.org/10.5194/gmd-9-2853-2016>, 2016.
- Joos, F., Bruno, M., Fink, R., Siegenthaler, U., Stocker, T. F., Le Quéré, C., and Sarmiento, J. L.: An efficient and accurate representation  
of complex oceanic and biospheric models of anthropogenic carbon uptake, Tellus, Series B: Chemical and Physical Meteorology, 48,  
397–417, <https://doi.org/10.1034/j.1600-0889.1996.t01-2-00006.x>, 1996.
- 950 Joos, F., Roth, R., Fuglestvedt, J. S., Peters, G. P., Enting, I. G., von Bloh, W., Brovkin, V., Burke, E. J., Eby, M., Edwards, N. R., Friedrich,  
T., Frölicher, T. L., Halloran, P. R., Holden, P. B., Jones, C., Kleinen, T., Mackenzie, F. T., Matsumoto, K., Meinshausen, M., Plattner, G.-  
K., Reisinger, A., Segschneider, J., Shaffer, G., Steinacher, M., Strassmann, K., Tanaka, K., Timmermann, A., and Weaver, A. J.: Carbon  
dioxide and climate impulse response functions for the computation of greenhouse gas metrics: a multi-model analysis, Atmospheric  
Chemistry and Physics, 13, 2793–2825, <https://doi.org/10.5194/acp-13-2793-2013>, 2013.
- K. Arora, V., Katavouta, A., Williams, R. G., Jones, C. D., Brovkin, V., Friedlingstein, P., Schwinger, J., Bopp, L., Boucher, O., Cadule, P.,  
955 Chamberlain, M. A., Christian, J. R., Delire, C., Fisher, A. R. A., Hajima, T., Ilyina, T., Joetzjer, E., Kawamiya, M., Koven, C. D., Krasting,  
J. P., Law, R. M., Lawrence, D. M., Lenton, A., Lindsay, K., Pongratz, J., Raddatz, T., Séférian, R., Tachiiri, K., Tjiputra, J. F., Wiltshire,  
A., Wu, T., and Ziehn, T.: Carbon-concentration and carbon-climate feedbacks in CMIP6 models and their comparison to CMIP5 models,  
Biogeosciences, 17, 4173–4222, <https://doi.org/10.5194/bg-17-4173-2020>, 2020.
- Kristiansen, N. I., Stohl, A., Olivié, D. J. L., Croft, B., Søvde, O. A., Klein, H., Christoudias, T., Kunkel, D., Leadbetter, S. J., Lee, Y. H.,  
960 Zhang, K., Tsigaridis, K., Bergman, T., Evangelou, N., Wang, H., Ma, P.-L., Easter, R. C., Rasch, P. J., Liu, X., Pitari, G., Di Genova, G.,  
Zhao, S. Y., Balkanski, Y., Bauer, S. E., Faluvegi, G. S., Kokkola, H., Martin, R. V., Pierce, J. R., Schulz, M., Shindell, D., Tost, H., and

- Zhang, H.: Evaluation of observed and modelled aerosol lifetimes using radioactive tracers of opportunity and an ensemble of 19 global models, *Atmospheric Chemistry and Physics*, 16, 3525–3561, <https://doi.org/10.5194/acp-16-3525-2016>, 2016.
- Lashof, D. A. and Ahuja, D. R.: Relative contributions of greenhouse gas emissions to global warming, *Nature*, 344, 529–531, 965 <https://doi.org/10.1038/344529a0>, 1990.
- Leach, N. J., Millar, R. J., Haustein, K., Jenkins, S., Graham, E., and Allen, M. R.: Current level and rate of warming determine emissions budgets under ambitious mitigation, *Nature Geoscience*, 11, 574–579, <https://doi.org/10.1038/s41561-018-0156-y>, 2018.
- Lee, D., Fahey, D., Skowron, A., Allen, M., Burkhardt, U., Chen, Q., Doherty, S., Freeman, S., Forster, P., Fuglestvedt, J., Gettelman, A., De León, R., Lim, L., Lund, M., Millar, R., Owen, B., Penner, J., Pitari, G., Prather, M., Sausen, R., and Wilcox, L.: 970 The contribution of global aviation to anthropogenic climate forcing for 2000 to 2018, *Atmospheric Environment*, 244, 117834, <https://doi.org/10.1016/j.atmosenv.2020.117834>, 2021.
- Lenssen, N. J. L., Schmidt, G. A., Hansen, J. E., Menne, M. J., Persin, A., Ruedy, R., and Zyss, D.: Improvements in the uncertainty model in the Goddard Institute for Space Studies Surface Temperature (GISSTEMP) analysis, *Journal of Geophysical Research: Atmospheres*, p. 2018JD029522, <https://doi.org/10.1029/2018JD029522>, 2019.
- 975 MacDougall, A. H.: The Transient Response to Cumulative CO<sub>2</sub> Emissions: a Review, <https://doi.org/10.1007/s40641-015-0030-6>, 2016.
- Marvel, K., Schmidt, G. A., Miller, R. L., and Nazarenko, L. S.: Implications for climate sensitivity from the response to individual forcings, *Nature Climate Change*, 6, 386–389, <https://doi.org/10.1038/nclimate2888>, 2016.
- Matthews, H. D., Gillett, N. P., Stott, P. A., and Zickfeld, K.: The proportionality of global warming to cumulative carbon emissions, *Nature*, 459, 829–832, <https://doi.org/10.1038/nature08047>, 2009.
- 980 Meinshausen, M., Meinshausen, N., Hare, W., Raper, S. C. B., Frieler, K., Knutti, R., Frame, D. J., and Allen, M. R.: Greenhouse-gas emission targets for limiting global warming to 2 °C, *Nature*, 458, 1158–1162, <https://doi.org/10.1038/nature08017>, 2009.
- Meinshausen, M., Raper, S. C. B., and Wigley, T. M. L.: Emulating coupled atmosphere-ocean and carbon cycle models with a simpler model, MAGICC6 – Part 1: Model description and calibration, *Atmospheric Chemistry and Physics*, 11, 1417–1456, <https://doi.org/10.5194/acp-11-1417-2011>, 2011a.
- 985 Meinshausen, M., Wigley, T. M. L., and Raper, S. C. B.: Emulating atmosphere-ocean and carbon cycle models with a simpler model, MAGICC6 – Part 2: Applications, *Atmospheric Chemistry and Physics*, 11, 1457–1471, <https://doi.org/10.5194/acp-11-1457-2011>, 2011b.
- Meinshausen, M., Vogel, E., Nauels, A., Lorbacher, K., Meinshausen, N., Etheridge, D. M., Fraser, P. J., Montzka, S. A., Rayner, P. J., Trudinger, C. M., Krummel, P. B., Beyerle, U., Canadell, J. G., Daniel, J. S., Enting, I. G., Law, R. M., Lunder, C. R., O'Doherty, S., Prinn, R. G., Reimann, S., Rubino, M., Velders, G. J. M., Vollmer, M. K., Wang, R. H. J., and Weiss, R.: Historical greenhouse gas concentrations for climate modelling (CMIP6), *Geoscientific Model Development*, 10, 2057–2116, <https://doi.org/10.5194/gmd-10-2057-2017>, 2017.
- 990 Meinshausen, M., Nicholls, Z., Lewis, J., Gidden, M., Vogel, E., Freund, M., Beyerle, U., Gessner, C., Nauels, A., Bauer, N., Canadell, J., Daniel, J., John, A., Krummel, P., Luderer, G., Meinshausen, N., Montzka, S., Rayner, P., Reimann, S., Smith, S., van den Berg, M., Velders, G., Vollmer, M., and Wang, H. J.: The SSP greenhouse gas concentrations and their extensions to 2500, *Geoscientific Model Development Discussions*, pp. 1–77, <https://doi.org/10.5194/gmd-2019-222>, 2019.
- Millar, R. J. and Friedlingstein, P.: The utility of the historical record for assessing the transient climate response to cumulative emissions, *Philosophical Transactions of the Royal Society of London A: Mathematical, Physical and Engineering Sciences*, 376, <https://doi.org/10.1098/rsta.2016.0449>, 2018.

- Millar, R. J., Otto, A., Forster, P. M., Lowe, J. A., Ingram, W. J., and Allen, M. R.: Model structure in observational constraints on transient  
1000 climate response, *Climatic Change*, 131, 199–211, <https://doi.org/10.1007/s10584-015-1384-4>, 2015.
- Millar, R. J., Nicholls, Z. R., Friedlingstein, P., and Allen, M. R.: A modified impulse-response representation of the global near-surface air  
temperature and atmospheric concentration response to carbon dioxide emissions, *Atmospheric Chemistry and Physics*, 17, 7213–7228,  
<https://doi.org/10.5194/acp-17-7213-2017>, 2017.
- Morice, C. P., Kennedy, J. J., Rayner, N. A., Jones, P. D., P., M. C., J., K. J., A., R. N., and D., J. P.: Quantifying uncertainties in global and  
1005 regional temperature change using an ensemble of observational estimates: The HadCRUT4 data set, *Journal of Geophysical Research: Atmospheres*, 117, <https://doi.org/10.1029/2011JD017187>, 2011.
- Morice, C. P., Kennedy, J. J., Rayner, N. A., Winn, J. P., Hogan, E., Killick, R. E., Dunn, R. J. H., Osborn, T. J., Jones, P. D., and Simpson,  
I. R.: An updated assessment of near-surface temperature change from 1850: the HadCRUT5 dataset, *Journal of Geophysical Research: Atmospheres*, <https://doi.org/10.1029/2019JD032361>, 2020.
- 1010 Myhre, G., Shindell, D., Bre' on, F.-M., Collins, W., Fuglestvedt, J., Huang, J., Koch, D., Lamarque, J.-F., Lee, D., Mendoza, B., Nakajima, T., Robock, A., Stephens, G., Takemura, T., and Zhang, H.: Anthropogenic and Natural Radiative Forcing, in: *Climate Change 2013: The Physical Science Basis. Contribution of Working Group I to the Fifth Assessment Report of the Intergovernmental Panel on Climate Change*, edited by Stocker, T. F., Qin, D., Plattner, G.-K., Tignor, M., Allen, S. K., Boschung, J., Nauels, A., Xia, Y., Bex, V., and Midgley, P. M., chap. 8, pp. 659–740, Cambridge University Press, Cambridge, United Kingdom and New York, NY, USA,  
1015 <https://doi.org/10.1017/CBO9781107415324.018>, 2013.
- Nelder, J. A. and Mead, R.: A Simplex Method for Function Minimization, *The Computer Journal*, 7, 308–313,  
<https://doi.org/10.1093/comjnl/7.4.308>, 1965.
- Newman, P. A., Daniel, J. S., Waugh, D. W., and Nash, E. R.: A new formulation of equivalent effective stratospheric chlorine (EESC),  
*Atmospheric Chemistry and Physics*, 7, 4537–4552, <https://doi.org/10.5194/acp-7-4537-2007>, 2007.
- 1020 Nicholls, Z., Meinshausen, M., Lewis, J., Gieseke, R., Dommenget, D., Dorheim, K., Fan, C.-S., Fuglestvedt, J., Gasser, T., Golüke, U.,  
Goodwin, P., Kriegler, E., Leach, N., Marchegiani, D., Quilcaille, Y., Samset, B., Sandstad, M., Shiklomanov, A., Skeie, R., Smith, C.,  
Tanaka, K., Tsutsui, J., and Xie, Z.: Reduced complexity model intercomparison project phase 1: Protocol, results and initial observations,  
*Geoscientific Model Development Discussions*, pp. 1–33, <https://doi.org/10.5194/gmd-2019-375>, 2020a.
- Nicholls, Z., Lewis, J., Makin, M., Nattala, U., Zhang, G. Z., Mutch, S. J., Tescari, E., and Meinshausen, M.: Regionally aggregated,  
1025 stitched and de-drifted CMIP-climate data, processed with netCDF-SCM v2.0.0, *Geoscience Data Journal*, 00, gdj3.113,  
<https://doi.org/10.1002/gdj3.113>, 2021.
- Nicholls, Z. R. J., Meinshausen, M. A., Lewis, J., Rojas Corradi, M., Dorheim, K., Gasser, T., Gieseke, R., Hope, A. P., Leach, N., McBride,  
L. A., and al., E.: Reduced Complexity Model Intercomparison Project Phase 2: Synthesising Earth system knowledge for probabilistic  
climate projections, *Earth and Space Science Open Archive*, p. 29, <https://doi.org/10.1002/ESSOAR.10504793.1>, 2020b.
- 1030 Nijssse, F. J. M. M., Cox, P. M., and Williamson, M. S.: Emergent constraints on transient climate response (TCR) and equilibrium  
climate sensitivity (ECS) from historical warming in CMIP5 and CMIP6 models, *Earth System Dynamics*, 11, 737–750,  
<https://doi.org/10.5194/esd-11-737-2020>, 2020.
- Prather, M. J., Holmes, C. D., and Hsu, J.: Reactive greenhouse gas scenarios: Systematic exploration of uncertainties and the role of  
atmospheric chemistry, *Geophysical Research Letters*, <https://doi.org/10.1029/2012GL051440>, 2012.

- 1035 Prather, M. J., Hsu, J., DeLuca, N. M., Jackman, C. H., Oman, L. D., Douglass, A. R., Fleming, E. L., Strahan, S. E., Steenrod, S. D., Søvde, O. A., Isaksen, I. S. A., Froidevaux, L., and Funke, B.: Measuring and modeling the lifetime of nitrous oxide including its variability, Journal of Geophysical Research: Atmospheres, 120, 5693–5705, <https://doi.org/10.1002/2015JD023267>, 2015.
- Ramaswamy, V., Boucher, O., Haigh, J., Hauglustaine, D., Haywood, J., Myhre, G., Nakajima, T., Shi, G., and Solomon, S.: Radiative Forcing of Climate Change, in: Climate Change 2001: The Scientific Basis. Contribution of Working Group I to the Third Assessment Report of the Intergovernmental Panel on Climate Change, edited by [Houghton, J.T., Y. D., Griggs, D., Noguer, M., van der Linden, P., Dai, X., Maskell, K., and Johnson, C., chap. 6, Cambridge University Press, Cambridge, United Kingdom and New York, NY, USA, 881pp, 2001.
- 1040 Riahi, K., Rao, S., Krey, V., Cho, C., Chirkov, V., Fischer, G., Kindermann, G., Nakicenovic, N., and Rafaj, P.: RCP 8.5—A scenario of comparatively high greenhouse gas emissions, Climatic Change, 109, 33–57, <https://doi.org/10.1007/s10584-011-0149-y>, 2011.
- 1045 Riahi, K., van Vuuren, D. P., Kriegler, E., Edmonds, J., O'Neill, B. C., Fujimori, S., Bauer, N., Calvin, K., Dellink, R., Fricko, O., Lutz, W., Popp, A., Cuarterma, J. C., KC, S., Leimbach, M., Jiang, L., Kram, T., Rao, S., Emmerling, J., Ebi, K., Hasegawa, T., Havlik, P., Humpenöder, F., Da Silva, L. A., Smith, S., Stehfest, E., Bosetti, V., Eom, J., Gernaat, D., Masui, T., Rogelj, J., Streffler, J., Drouet, L., Krey, V., Luderer, G., Harmsen, M., Takahashi, K., Baumstark, L., Doelman, J. C., Kainuma, M., Klimont, Z., Marangoni, G., Lotze-Campen, H., Obersteiner, M., Tabeau, A., and Tavoni, M.: The Shared Socioeconomic Pathways and their energy, land use, and greenhouse gas emissions implications: An overview, Global Environmental Change, 42, 153–168, <https://doi.org/10.1016/J.GLOENVCHA.2016.05.009>, 2017.
- 1050 Ribes, A., Qasmi, S., and Gillett, N. P.: Making climate projections conditional on historical observations, Science Advances, 7, eabc0671, <https://doi.org/10.1126/sciadv.abc0671>, 2021.
- Richardson, M., Cowtan, K., Hawkins, E., and Stolpe, M. B.: Reconciled climate response estimates from climate models and the energy budget of Earth, Nature Climate Change, 6, 931–935, <https://doi.org/10.1038/nclimate3066>, 2016.
- 1055 Richardson, M., Cowtan, K., and Millar, R. J.: Global temperature definition affects achievement of long-term climate goals, Environmental Research Letters, 13, 54 004, <https://doi.org/10.1088/1748-9326/aab305>, 2018.
- Rohde, R., Muller, R. A., Jacobsen, R., Muller, E., Perlmutter, S., Rosenfeld, A., Wurtele, J., Groom, D., and Wickham, C.: A New Estimate of the Average Earth Surface Land Temperature Spanning 1753 to 2011, Geoinformatics & Geostatistics: An Overview, 1, 1, <https://doi.org/10.4172/2327-4581.1000101>, 2013.
- 1060 Rugenstein, M., Bloch-Johnson, J., Gregory, J., Andrews, T., Mauritsen, T., Li, C., Frölicher, T. L., Paynter, D., Danabasoglu, G., Yang, S., Dufresne, J., Cao, L., Schmidt, G. A., Abe-Ouchi, A., Geoffroy, O., and Knutti, R.: Equilibrium Climate Sensitivity Estimated by Equilibrating Climate Models, Geophysical Research Letters, 47, <https://doi.org/10.1029/2019GL083898>, 2020.
- Sanderson, B.: Relating climate sensitivity indices to projection uncertainty, Earth System Dynamics, 11, 721–735, <https://doi.org/10.5194/esd-11-721-2020>, 2020.
- 1065 Sherwood, S., Webb, M. J., Annan, J. D., Armour, K. C., Forster, P. M., Hargreaves, J. C., Hegerl, G., Klein, S. A., Marvel, K. D., Rohling, E. J., Watanabe, M., Andrews, T., Braconnot, P., Bretherton, C. S., Foster, G. L., Hausfather, Z., von der Heydt, A. S., Knutti, R., Mauritsen, T., Norris, J. R., Proistosescu, C., Rugenstein, M., Schmidt, G. A., Tokarska, K. B., and Zelinka, M. D.: An assessment of Earth's climate sensitivity using multiple lines of evidence, Reviews of Geophysics, <https://doi.org/10.1029/2019rg000678>, 2020.
- 1070 Skeie, R. B., Myhre, G., Hodnebrog, Ø., Cameron-Smith, P. J., Deushi, M., Hegglin, M. I., Horowitz, L. W., Kramer, R. J., Michou, M., Mills, M. J., Olivié, D. J., Connor, F. M., Paynter, D., Samset, B. H., Sellar, A., Shindell, D., Takemura, T., Tilmes, S., and Wu, T.: Historical total

- ozone radiative forcing derived from CMIP6 simulations, *npj Climate and Atmospheric Science*, 3, 1–10, <https://doi.org/10.1038/s41612-020-00131-0>, 2020.
- Smith, C.: Effective Radiative Forcing Time Series from the Shared Socioeconomic Pathways, <https://doi.org/10.5281/ZENODO.3973015>, 1075 2020.
- Smith, C. J., Forster, P. M., Allen, M., Leach, N., Millar, R. J., Passerello, G. A., and Regayre, L. A.: FAIR v1.3: a simple emissions-based impulse response and carbon cycle model, *Geoscientific Model Development*, 11, 2273–2297, <https://doi.org/10.5194/gmd-11-2273-2018>, 2018.
- Smith, C. J., Harris, G., Palmer, M. D., Bellouin, N., Myhre, G., Schulz, M., Golaz, J.-C., Ringer, M., Storelvmo, T., and Forster, P. M.: Energy 1080 Budget Constraints on the Time History of Aerosol Forcing and Climate Sensitivity, *Journal of Geophysical Research: Atmospheres*, in submiss, <https://doi.org/10.1002/ESSOAR.10503977.2>, 2020.
- Stevenson, D. S., Young, P. J., Naik, V., Lamarque, J.-F., Shindell, D. T., Voulgarakis, A., Skeie, R. B., Dalsoren, S. B., Myhre, G., Berntsen, 1085 T. K., Folberth, G. A., Rumbold, S. T., Collins, W. J., MacKenzie, I. A., Doherty, R. M., Zeng, G., van Noije, T. P. C., Strunk, A., Bergmann, D., Cameron-Smith, P., Plummer, D. A., Strode, S. A., Horowitz, L., Lee, Y. H., Szopa, S., Sudo, K., Nagashima, T., Josse, B., Cionni, I., Righi, M., Eyring, V., Conley, A., Bowman, K. W., Wild, O., and Archibald, A.: Tropospheric ozone changes, radiative forcing and attribution to emissions in the Atmospheric Chemistry and Climate Model Intercomparison Project (ACCMIP), *Atmospheric Chemistry and Physics*, 13, 3063–3085, <https://doi.org/10.5194/acp-13-3063-2013>, 2013.
- Taylor, K. E., Stouffer, R. J., and Meehl, G. A.: An Overview of CMIP5 and the Experiment Design, *Bulletin of the American Meteorological Society*, 93, 485–498, <https://doi.org/10.1175/BAMS-D-11-00094.1>, 2012.
- 1090 Thornhill, G. D., Collins, W. J., Kramer, R. J., Olivie, D., Skeie, R. B., O'Connor, F. M., Abraham, N. L., Checa-Garcia, R., Bauer, S. E., Deushi, M., Emmons, L. K., Forster, P. M., Horowitz, L. W., Johnson, B., Keeble, J., Lamarque, J.-F., Michou, M., Mills, M. J., Mulcahy, J. P., Myhre, G., Nabat, P., Naik, V., Oshima, N., Schulz, M., Smith, C. J., Takemura, T., Tilmes, S., Wu, T., Zeng, G., and Zhang, J.: Effective radiative forcing from emissions of reactive gases and aerosols – a multi-model comparison, *Atmospheric Chemistry and Physics*, 21, 853–874, <https://doi.org/10.5194/acp-21-853-2021>, 2021.
- 1095 Tokarska, K. B., Schleussner, C.-F., Rogelj, J., Stolpe, M. B., Matthews, H. D., Pfleiderer, P., and Gillett, N. P.: Recommended temperature metrics for carbon budget estimates, model evaluation and climate policy, *Nature Geoscience*, 12, 964–971, <https://doi.org/10.1038/s41561-019-0493-5>, 2019.
- Tokarska, K. B., Stolpe, M. B., Sippel, S., Fischer, E. M., Smith, C. J., Lehner, F., and Knutti, R.: Past warming trend constrains future warming in CMIP6 models, *Science Advances*, 6, 9549–9567, <https://doi.org/10.1126/sciadv.aaz9549>, 2020.
- 1100 Trenberth, K. E. and Fasullo, J. T.: An apparent hiatus in global warming?, *Earth's Future*, 1, 19–32, <https://doi.org/10.1002/2013ef000165>, 2013.
- Tsutsui, J.: Quantification of temperature response to CO<sub>2</sub> forcing in atmosphere–ocean general circulation models, *Climatic Change*, 140, 287–305, <https://doi.org/10.1007/s10584-016-1832-9>, 2017.
- Tsutsui, J.: Diagnosing Transient Response to CO<sub>2</sub> Forcing in Coupled Atmosphere-Ocean Model Experiments Using a Climate Model 1105 Emulator, *Geophysical Research Letters*, 47, <https://doi.org/10.1029/2019GL085844>, 2020.
- Velders, G. J. and Daniel, J. S.: Uncertainty analysis of projections of ozone-depleting substances: Mixing ratios, EESC, ODPs, and GWPs, *Atmospheric Chemistry and Physics*, 14, 2757–2776, <https://doi.org/10.5194/acp-14-2757-2014>, 2014.
- Vose, R. S., Arndt, D., Banzon, V. F., Easterling, D. R., Gleason, B., Huang, B., Kearns, E., Lawrimore, J. H., Menne, M. J., Peterson, T. C., Reynolds, R. W., Smith, T. M., Williams, C. N., Wuertz, D. B., Vose, R. S., Arndt, D., Banzon, V. F., Easterling, D. R., Gleason,

- 1110 B., Huang, B., Kearns, E., Lawrimore, J. H., Menne, M. J., Peterson, T. C., Reynolds, R. W., Smith, T. M., Jr., C. N. W., and Wuertz,  
D. B.: NOAA's Merged Land–Ocean Surface Temperature Analysis, *Bulletin of the American Meteorological Society*, 93, 1677–1685,  
<https://doi.org/10.1175/BAMS-D-11-00241.1>, 2012.
- Wilks, D. S.: Resampling hypothesis tests for autocorrelated fields, *Journal of Climate*, 10, 65–82, [https://doi.org/10.1175/1520-0442\(1997\)010<0065:RHTFAF>2.0.CO;2](https://doi.org/10.1175/1520-0442(1997)010<0065:RHTFAF>2.0.CO;2), 1997.
- 1115 Zelinka, M. D., Andrews, T., Forster, P. M., and Taylor, K. E.: Quantifying components of aerosol-cloud-radiation interactions in climate  
models, *Journal of Geophysical Research: Atmospheres*, 119, 7599–7615, <https://doi.org/10.1002/2014JD021710>, 2014.
- Zickfeld, K., MacDougall, A. H., and Matthews, H. D.: On the proportionality between global temperature change and cumulative CO  
<sub>2</sub> emissions during periods of net negative CO <sub>2</sub> emissions, *Environmental Research Letters*, 11, 055006,  
<https://doi.org/10.1088/1748-9326/11/5/055006>, 2016.